ERS-2 Wind Scatterometer
Cyclic Report

From 27th December 2010 to 31st January 2011
Cycle 164

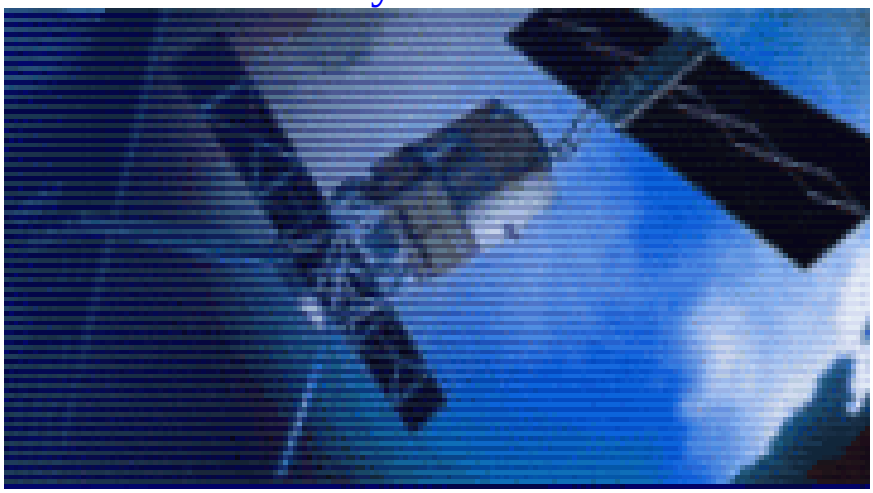

Prepared by: M. Talone (scat@eo-sppa.org)

Inputs from: G. De Chiara (ECMWF)

Issue: 1.0
Reference ERSE-SPPA-EOPG-TN-10-0010
Date of issue: 1st April 2011
Document type: Technical Note

Table of Content

1 Introduction and Summary 3
2 Calibration Performances 6
2.1 Gain Constant over transponder 6
2.2 Ocean Calibration 6
2.3 Gamma-nought over the Brazilian rain forest 9
2.4 Antenna pattern: Gamma-nought as a function of elevation angle 9
2.5 Antenna pattern: Gamma-nought as a function of incidence angle 10
2.6 Gamma nought histograms and peak position evolution 11
2.7 Gamma nought image of the reference area 12
2.8 Sigma nought evolution 13
2.9 Antenna temperature evolution over the Rain Forest 13
3 Instrument performance 14
3.1 Centre of gravity and standard deviation of received power spectrum 14
3.2 Noise power level I and Q channel 22
3.3 Power level of internal calibration pulse 26
4 Products performance 29
4.1 Products availability 29
4.2 PCS Geophysical Monitoring 36
4.3 ECMWF Geophysical Monitoring 41
4.3.1 Distance to cone history 44
4.3.2 UWI minus First-Guess history 46
4.3.3 Scatter plots 52
4.4 Timeliness evolution 57
5 Yaw error angle estimation 60
5.1 Degraded Scatterometer Measurements 64

1 Introduction and Summary

The document includes a summary of the daily quality control made within the IDEAS (Instrument Data quality Evaluation and Analysis Service) and various sections describing the results of the investigations and studies of "open-problems" related to the Scatterometer. In each section results are shown from the beginning of the mission in order to see the evolution and to outline possible "seasonal" effects. An explanation for the major events which have impacted the performance since launch is given, and comments about the recent events which occurred during the last cycle are included.
This report covers the period from 27th December 2010 to 31st January 2011 (cycle 164) and includes the results of the monitoring activity performed by ESRIN and ECMWF. This document is available on line at: http://earth.esa.int/pcs/ers/scatt/reports/pcs_cyclic/

Mission events

The following bullets summarize the major mission facts for cycle 164:

- The ERS-2 satellite was piloted in ZGM throughout the cycle.
- The ESACA processor worked nominally without faults.
- Missing data from Johannesburg station from 16th December 2008 onwards due to ground station hardware failure.
- Missing data from Singapore station from 30th December 2009 onwards due to a ground station facility problem.
- Missing data from Beijing station from 27th June 2010 onwards due to a ground station hardware failure.
- Missing data from Mcmurdo station from 15th November 2010 due to a ground station maintenance activity.
- Missing data from Hobart station from 11th November 2010 due to ground station problems.
- Missing data from Chetumal station from 9th to 18th January 2011.
- Missing data from Miami station on 4th and 10th January 2011.
- A planned manoeuvre was performed on 7th January 2011. During the manoeuvre data accuracy could be degraded. The user can filter out that data set by checking the Doppler and yaw quality flag inside the UWI product or the combined Kp-Yaw flag for the BUFR product.
- On 4th January 2011 AMI was set to HEATER mode in preparation for eclipse, as a consequence data were missed from 8:03:00 to 9:13:13 and from 9:44:00 to 10:27:10.
- For the entire period of cycle 164, ERS-2 Scatterometer data was used in the 4D-Var data

assimilation system at ECMWF.

News on the ERS mission is available on line: http://earth.esa.int/ers/new_ers_news.html

Data Coverage

After the on board tape recorder failure in July 2003, data is acquired in real time whenever within the visibility range of a ground station. The coverage at the west coast of the US and Canada is lower and sparser for the descending orbits with respect to the ascending ones due to the lack of acquisitions from Prince Albert and Gatineau stations at those passes. For Cycle 164, data coverage was over the North-Atlantic, the Mediterranean, part of the Gulf of Mexico, an area in the Pacific west from the US, Canada and Central America and some data over the area in between Antarctica and Australia. In this latter region coverage was reduced with respect to Cycle 163, due to the lack of acquisitions from Hobart and McMurdo ground stations.

Yaw performance

The result of the monitoring for cycle 164 is an average (per orbit) yaw error angle within the expected nominal range (+/- 2 degrees).

Calibration performance

- Calibration using transponders has been interrupted since January 2001. Data from the transponders were acquired until January 2005 and will be used in the next reprocessing. In January 2005, due to a system failure, transponders were switched down. Since September 2010, the Calibration Mode has been removed from the satellite orbital planning and substituted by nominal acquisition.
- The calibration monitoring over the Brazilian rain forest has been reactivated since cycle 148. Despite the limited coverage, the monitoring is still valid for ascending passes. In the reporting period no data is available at descending passes due to limited acquisition caused by problems occurred to the ground stations. From the data analyzed no signal degradations have been observed and that the calibration stability is within the geophysical noise.
- The Ocean Calibration monitoring is performed by ECMWF. The average backscatter bias levels was less negative (-0.48 dB, was -0.54 dB), being 0.1 dB more negative than for nominal data in 2000 (around -0.4 dB; see Figure 1 of the reports for Cycle 48 to 59). The asymmetry is slightly worse than that of one year ago (see report for Cycle 152). Long-term

variations correlate with the yearly cycle, which, given the non-global coverage, is understandable. Therefore, the method of ocean calibration will probably only provide accurate information on calibration levels for globally or yearly averaged data sets.

Instrument performance

• During the cycle 164 the mean transmitted power evolution had a mean decreasing trend of 0.03 dB. This value is lower than the nominal decreasing trend of 0.1 dB/Cycle detected since the beginning of the mission.
• The evolution of the noise power during the cycle 164 was stable. The daily average for the Fore and Aft beam noise is around 1.7 ADC (I) and around 1.6 ADC (Q), respectively. For the Mid beam the noise is around 1.2 ADC both I and Q.
• During the cycle 164 the Doppler compensation evolution was stable. The daily average of the CoG of the compensated received signal is around 60 Hz and -10 Hz for the Fore and Aft antenna respectively. For the Mid antenna it was around 240 Hz. The standard deviation of the CoG was around 1500 Hz for the Fore and Aft antenna and around 2700 Hz for the Mid antenna.

Timeliness performance

During cycle 164 the timeliness performances stayed stable for most of the stations. In the reporting period Kiruna showed the lowest timeliness of 30 minutes, Maspalomas, Gatineau. Miami, Chetumal, and Matera had a mean value of about 40 minutes. West Freugh's timeliness was about 50 minutes. No relevant information on Johannesburg, Singapore, McMurdo, Hobart, and Beijing stations due to missing data for the reporting period.

Product performance

During Cycle 164 data was received between 21:05 UTC 27 December 2010 and 20:59 UTC 31 January 2011. Data was grouped into 6-hourly batches (centred around 00, 06, 12 and 18 UTC). For all batches data was received.

Compared to Cycle 163, the UWI wind speed relative to ECMWF first-guess (FG) fields showed a slightly higher standard deviation (1.52 m/s, was 1.48 m/s). Bias levels were a bit more negative (on average -0.86 m/s, was -0.84 m/s). Relative standard deviation for wind

direction has improved (28.9 degrees, was 33.0 degrees).

The PCS geophysical monitoring reports a wind speed bias (UWI vs 18 or 24 hour forecast) of 0.7 m/s and a speed bias standard deviation around 1.8 m/s.

The wind direction deviation for cycle 164 was good with more than 98% of the nodes wind direction in agreement with the ECMWF forecast.

2 Calibration Performances

The calibration performances are estimated using three types of target: a man made target (the transponder) and two natural targets (the rain forest and the ocean). This approach allow us to design the correct calibration using a punctual but accurate information from transponders and an extended but noisy information from rain forest and ocean for which the main component of the variance comes from the geophysical evolution of the natural target and from the backscattering models used. These aspects are in the calibration performance monitoring philosophy. The major goals of the calibration monitoring activities are the achievement of a “flat” antenna pattern profile and the assurance of a stable absolute calibration level.

2.1 Gain Constant over transponder

One gain constant is computed per transponder per beam from the actual and simulated two-dimensional echo power, which is given as a function of the orbit time and range time. This parameter clearly indicates the difference between “real instrument” and the mathematic model. In order to acquire data over the transponder the Scatterometer must be set in an appropriate operational mode defined as “Calibration Mode”. Calibration using transponders has been interrupted since January 2001. Data from the transponders were acquired until January 2005 and will be used in the next reprocessing. In January 2005, due to a system failure, transponders were switched down. Since September 2010, the Calibration Mode has been removed from the satellite orbital planning and substituted by nominal acquisition.

2.2 Ocean Calibration

The average sigma0 bias levels (compared to simulated sigma0's based on ECMWF model FG winds) stratified with respect to antenna beam, ascending or descending track and as

function of incidence angle (i.e. across-node number) is displayed in Figure 1.

Ocean calibration shows that inter-node and inter-beam dependencies between the fore and aft beam are similar. Average bias level was less negative (-0.48 dB, was -0.54 dB), being 0.1 dB more negative than for nominal data in 2000 (around -0.4 dB; see Figure 1 of the reports for Cycle 48 to 59). The asymmetry is slightly worse than that of one year ago (see report for Cycle 152).

Long-term variations correlate with the yearly cycle, which, given the non-global coverage, is understandable. Therefore, the method of ocean calibration will probably only provide accurate information on calibration levels for globally or yearly averaged data sets.

The data volume of descending tracks was about 33% lower than for ascending tracks.

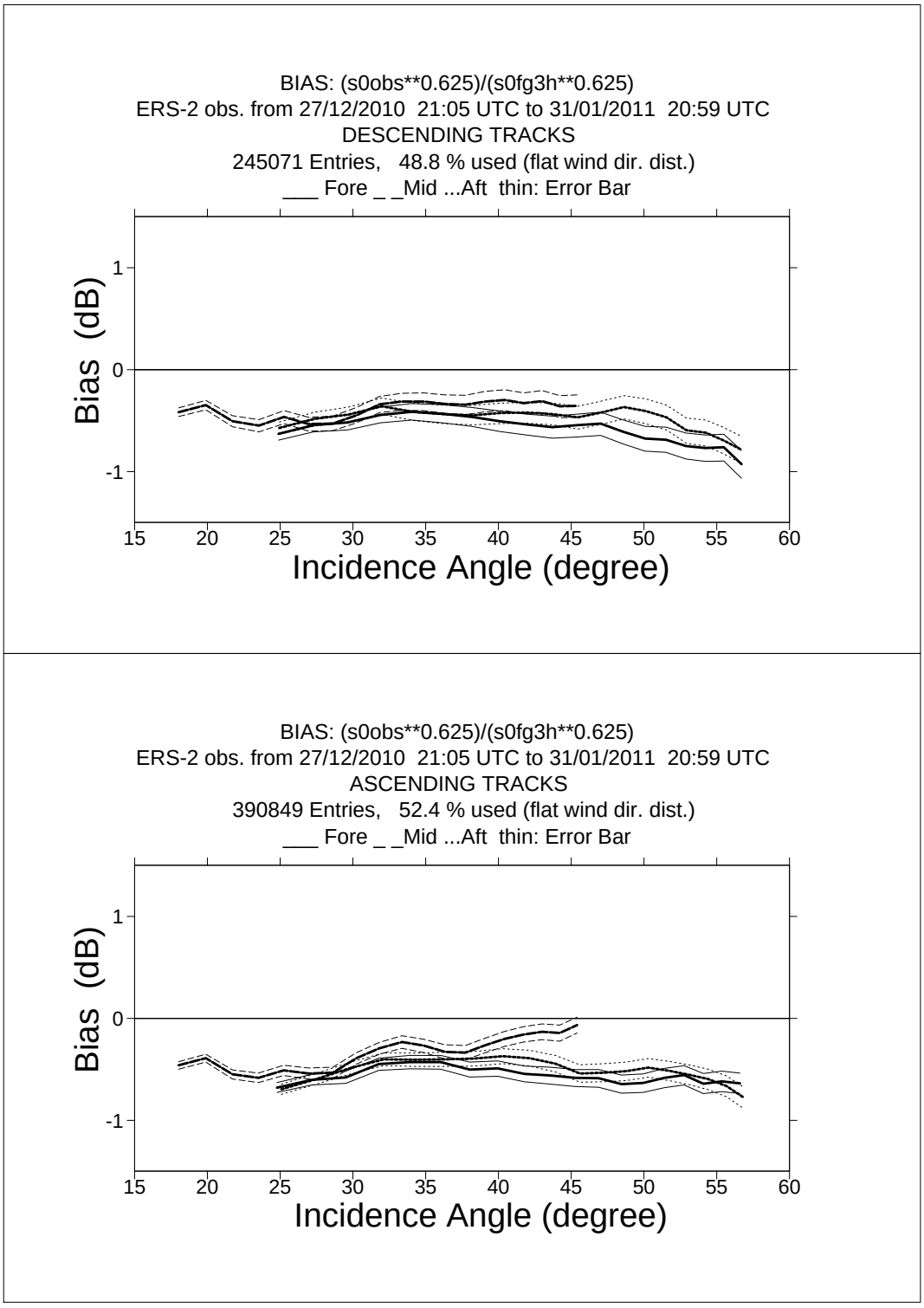

FIGURE 1 ERS-2 Scatterometer Ocean Calibration cycle 164. of <sigma_0^0.625>/<CMOD4(First Guess)^0.625> converted in dB for the fore beam (solid line), mid beam (dashed line) and aft beam (dotted line), as a function of incidence angle for descending and ascending tracks. The thin lines indicate the error bars on the estimated mean. First-guess winds are based on the in time closest (+3h, +6h, +9h, or +12h) T799 forecast field, and are bilinearly interpolated in space.

2.3 Gamma-nought over the Brazilian rain forest

Although the transponders give accurate measurements of the antenna attenuation at particular points of the antenna pattern, they are not adequate for fine tuning across all incidence angles, as there are simply not enough samples. The tropical rain forest in South America has been used as a reference distributed target. The target at the working frequency (C-band) of ERS-2 Scatterometer acts as a very rough surface, and the transmitted signal is equally scattered in all directions (the target is assumed to follow the isotropic approximation). Consequently, for the angle of incidence used by ERS-2 Scatterometer, the normalized backscattering coefficient (sigma nought) will depend solely on the surface effectively seen by the instrument:

$$S^0 = S \bullet \cos\theta$$

With this hypothesis it is possible to define the following formula:

$$\gamma^0 = \frac{\sigma^0}{\cos\theta}$$

Using the above equation, the gamma nought backscattering coefficient over the rain forest is independent of the incident angle, allowing the measurements from each of the three beams to be compared.
The test area used by the PCS is located between 2.5 degrees North and 5.0 degrees south in latitude and 60.5 degrees West and 70.0 degrees West in longitude.

That area was not covered at the beginning of the Regional Mission Scenario and therefore the calibration monitoring was suspended since cycle 86.
In February 2005 and October 2007 two ground stations have been put into operations, respectively in Miami and Chetumal, which partially cover the Rain Forest area. In the light of this current scenario, a new strategy has been assessed in order to re-activate the calibration performance monitoring. The investigation performed confirmed that with the current limited coverage the calibration monitoring is still valid for the Fore beam at descending passes and for Mid and Aft beams at ascending passes.
The calibration monitoring has been re-activated since the Cycle 148.

2.4 Antenna pattern: Gamma-nought as a function of elevation angle

For Cycle 164, the antenna patterns in function of the elevation angle have not been

computed by ESTEC.

2.5 Antenna pattern: Gamma-nought as a function of incidence angle

Due to the further reduced amount of data available during the reporting period, the antenna pattern has been computed by processing the last 3 cycles of data.

At ascending passes the antenna pattern for the Mid and Aft beams is quite similar to the one obtained before the degradation attitude occurred during cycle 60. The antenna pattern shows a flat profile, within 0.5 dB. For the Fore beam the limited amount of data results in a less flat profile at far range.
At descending passes the antenna pattern for the Fore and Mid Beams show a quite flat profile within 0.5 dB. Degradation for the Aft beam is due to limited amount of data.

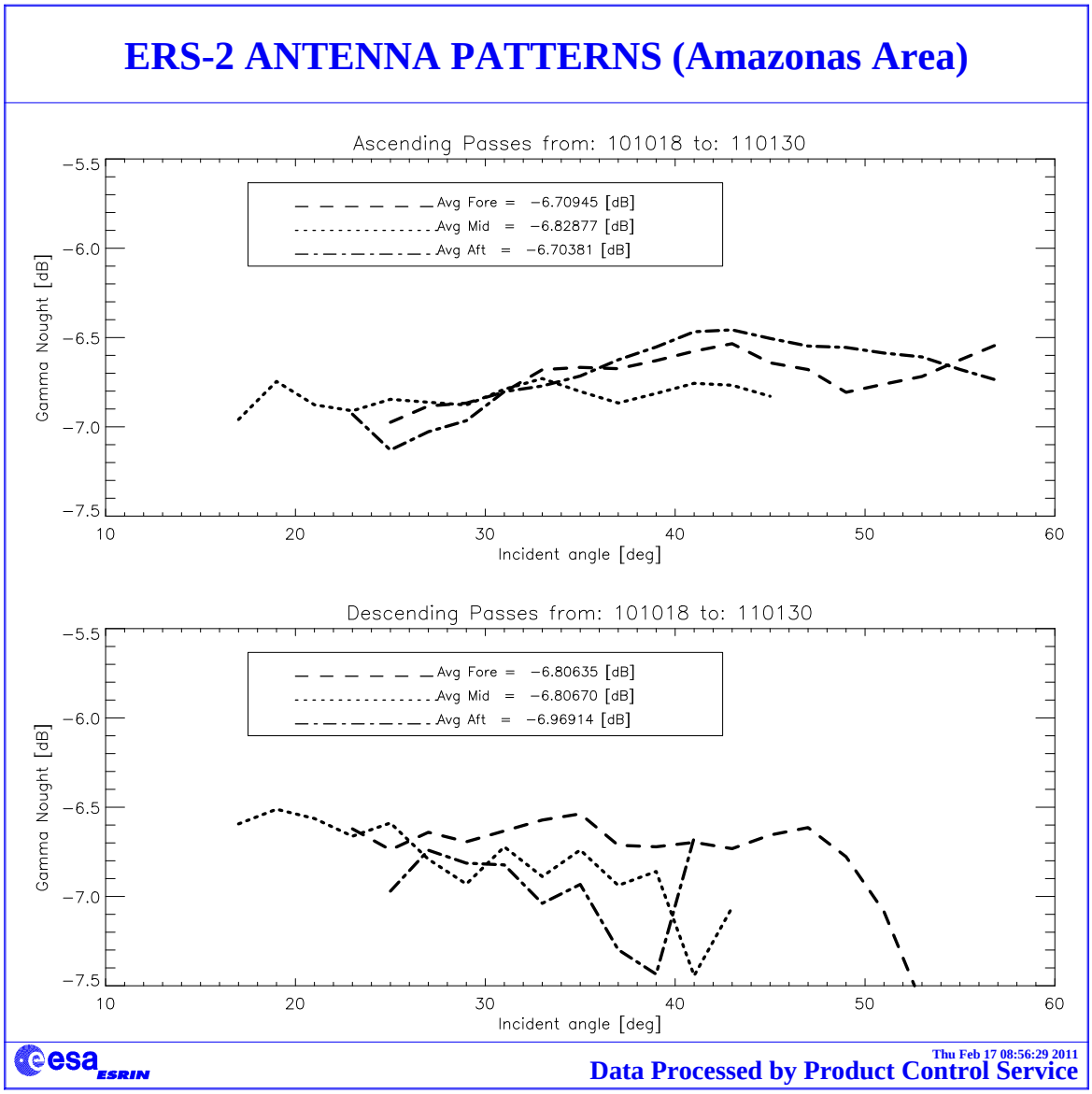

FIGURE 2 ERS-2 Scatterometer antenna pattern as function of the incidence angle: cycle 162, 163 and 164.

2.6 Gamma nought histograms and peak position evolution

As the gamma nought is independent from the incidence angle, the histogram of gamma nought over the rain forest is characterized by a sharp peak. The time-series of the peak position gives some information on the stability of the calibration. This parameter is computed by fitting the histogram with a normal distribution added to a second order polynomial:

$$F(x) = A_0 \cdot \exp\left(-\frac{z^2}{2}\right) + A_3 + A_4 \cdot x + A_5 \cdot x^2$$

where: $z = \frac{x - A_1}{A_2}$

The parameters are computed using a non linear least square method called “gradient expansion”. The position of the peak is given by the maximum of the function F(x).

The histograms are cyclic computed for each antenna individually “Fore”, “Mid” and “Aft” and for ascending and descending passes with a bin size of 0.02 dB.
Figure 3 shows the gamma nought histogram over the Brazilian rain forest throughout cycle 164.

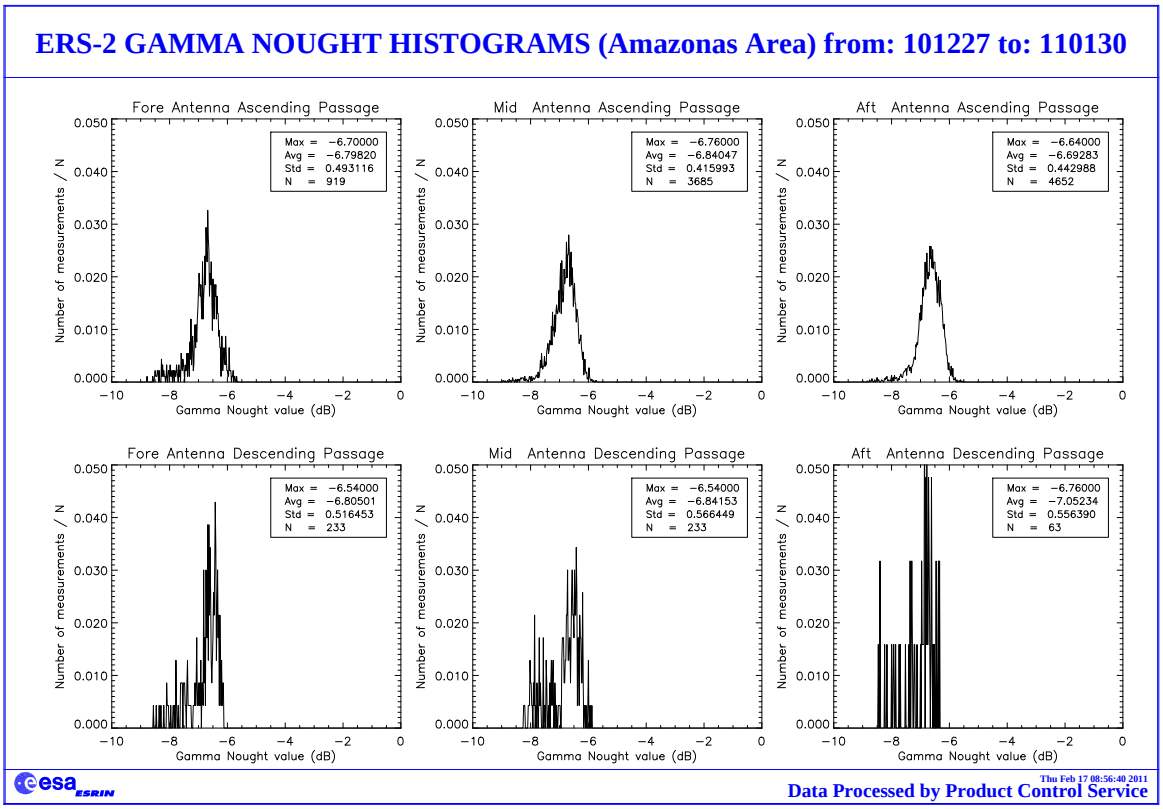

FIGURE 3 Gamma nought histograms over the Brazilian Rain Forest: cycle 164.

Due to the limited coverage of the reference area, data is mainly available for Mid and Aft beam at ascending passes and for Fore and Mid at descending passes. The histograms show a poor quality due to the limited amount of data.

2.7 Gamma nought image of the reference area

Figure 4 shows maps of the gamma nought over the Brazilian rain forest. This is the area where statistics are computed. Each map has a resolution of 0.5 degrees in latitude and 0.5 degrees in longitude; roughly this is the instrument resolution at the latitude of the test site. In

each resolution cell falls the average of all the valid observations available during the last 3 cycles (162, 163 and 164). Red area is used for no data cells.

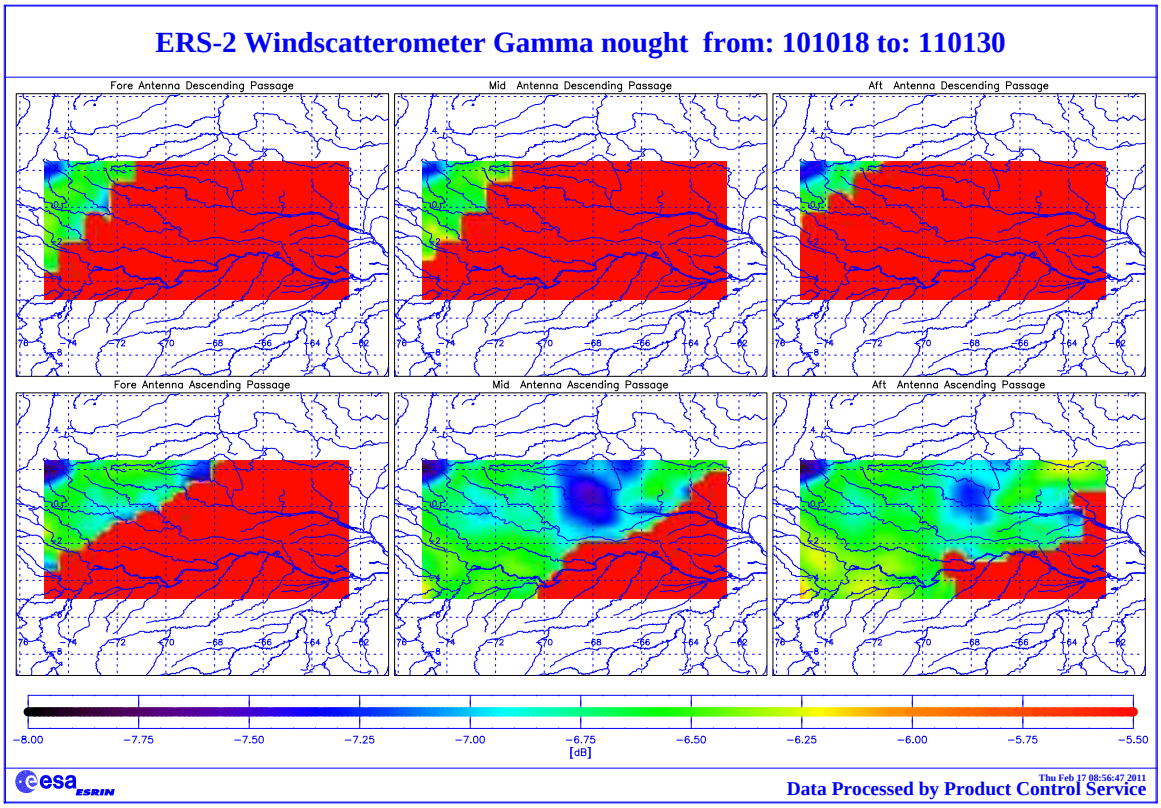

FIGURE 4 : ERS-2 Scatterometer: gamma nought over the Brazilian rain forest cycles 162, 163 and 164.

Due to the Regional Mission Scenario limited data is available for the three beams at descending passes; Mid and Aft beam data is available at Ascending passes. Despite the reduced amount of data, areas with low level of signals seem to be the same of the last cycles analyzed (till cycle 85).

2.8 Sigma nought evolution

The sigma nought evolution is not available for cycle 164.

2.9 Antenna temperature evolution over the Rain Forest

The antenna temperature evolution over the Rain Forest is not available for cycle 164.

3 Instrument performance

The instrument status is checked by monitoring the following parameters:

• Centre of Gravity (CoG) and standard deviation of the received signal spectrum after the on-ground Doppler Compensation filter. This parameter is useful for the monitoring of the orbit stability, the performances of the Doppler compensation filter, the behavior of the yaw steering mode and the performances of the devices in charge for the satellite attitude (e.g. gyroscopes, Earth sensor, Sun sensor).

• Noise power I and Q channel.

• Internal calibration pulse power.

The latter is an important parameter to monitor the transmitter and receiver chain, the evolution of pulse generator, the High Power Amplifier (HPA), the Traveling Wave Tube (TWT) and the receiver. These parameters are extracted daily from the UWI products and averaged. The evolution of each parameter is characterized by a least square line fit. The coefficients of the line fit are printed in each plot.

3.1 Centre of gravity and standard deviation of received power spectrum

The Figure 5 shows the evolution of the two parameters for each beam since the beginning of the ERS-2 mission and Figure 6 shows the same evolution only for the cycle 164.

The tendency during the nominal Yaw Steering Mode (YSM) period (beginning of the mission since the operation with the Mono Gyro (MGM) Attitude On-board Control System (AOCS) configuration on 7th February 2000) is a small and regular increase of the Centre of gravity (CoG) of received spectrum for the three antennae. During the YSM, two small changes can be detected in the CoG evolution. The first change is from 24th, January 1996 to 14th, March 1996, the second one is from 14th February 1997 to 22nd April 1997. The reason was a change in the pointing subsystem (DES reconfiguration) side B instead of side A after a depointing anomaly (see table 1 for the list of the all AOCS depointing anomaly occurred during the ERS-2 mission). During these periods side B was switched on. It is important to note that during the first time a clear difference in the CoG of the received spectrum is present only for the Fore antenna (an increase of roughly 100 Hz) while during the second time the change has affected all the three antennae (roughly an increase of 200 Hz, 50 Hz and

50 Hz for the fore, mid and aft antenna respectively).

At the beginning of 2000 the nominal 3-gyroes AOCS configuration (plus one Digital Earth Sensor -DES, and one Digital Sun Sensor -DSS and backups) was no more considered safe because 3 of the six gyros on-board were out of order or very noisy. For that reason the MGM was implemented as default piloting mode. The MGM configuration was designed to pilot the ERS-2 using only one gyro plus the DES and the DSS modules. Scope of ZGM configuration was to extend the satellite lifetime by using the available gyros one at the time.
With the MGM, an increase of roughly 200 Hz was observed at the end of the qualification period. After the AOCS commissioning phase this parameter further evolved within the nominal range with a negligible impact on the data quality.
In MGM configuration, the gyro 5 was used until 7th October 2000 when it failed. From 10th October 2000 to 24th October 2000 the gyro 6 was used. This explains the decrease of roughly 100Hz in the CoG of the received spectrum. From 25th October 2000 to 17th January 2001 the gyro 1 was used to pilot the ERS-2 satellite. On 17th January 2001 the AOCS was upgraded. The new configuration allows piloting the satellite without gyroscopes. Unfortunately a failure of the Digital Earth Sensor (DES A-side) caused ERS-2 to enter in Safe-Mode on the same day. On 25th January 2001 gyro #1 also failed.
Satellite attitude was recovered on 5th February 2001 with a coarse attitude control mode (EBM). During the period of safe mode the spacecraft had drifted out of the nominal dead band by some 30 Km. The nominal orbit was reached on 6th February 2001.
The EBM mode had a strong negative impact on the Scatterometer data quality and the dissemination of data products to end users was discontinued.

After that a series of AOCS upgrades has been implemented in order to improve the satellite attitude: on 30th March 2001 the Yaw steering law was re-introduced into the piloting function and on 7th June 2001 the Zero Gyro Mode (ZGM) has been implemented as nominal piloting mode. In ZGM the satellite attitude had an improvement in particular for the pitch and yaw error angle. This explains the reduction of the fluctuation in the received signal.
The CoG returns within its nominal value in February 2003 when the new ERS Scatterometer ground processor (ESACA) was put in operation (only for validation purposes) in Kiruna station. ESACA is able to compensate for errors in satellite attitude and to produce calibrated sigma noughts.
The evolution of the standard deviation of the CoG of the received spectrum was stable during the YSM phase. Small peaks are related with the events listed in Table 2. In MGM the evolution was within the nominal range while for the initial phase of the ZGM the performance was strong degraded. This because the on-ground Doppler filters was not able to

compensate for the satellite degraded attitude. The introduction of the ESACA processor in February 2003 cured the problem.

On 8th December 2006 10:43 p.m. to 9th December 2006 07:18 anomaly in the on board Doppler Compensation occurred. That did not impact on the evolution of the CoG because the ESACA ground processor has compensated the receiver signal for the Doppler frequency shift. The Scat Team has carried out a deep analysis of the anomaly (see the technical note OSME-DPQC-SEDA-TN-06-0328 for further details).

TABLE 1 ERS-2 Scatterometer AOCS depointing anomaly list

Start of the anomaly			**End of the anomaly**			**Remarks**
24th January	1996	9:10 a.m.	26thJanuary	1996	6:53 p.m.	AOCS depointing anomaly
14th February	1997	1:25 a.m.	15thFebruary	1997	3:44 p.m.	AOCS depointing anomaly
3rd June	1998	2:43 p.m.	6th June	1998	12:47 a.m.	AOCS depointing anomaly
1st September	1999	8:50 a.m.	2nd September	1999	1:28 a.m.	
7th October	2000	4:38 p.m.	10th October	2000	4:49 p.m	depointing anomaly gyro 5 failure
24th October	2000	4:05 p.m.	25th October	2000	12:05 p.m.	depointing anomaly gyro 6 failure
17th January	2001		5th February	2001		gyro 1 failure Satellite in safe mode

TABLE 2 ERS-2 Scatterometer anomalies in the Doppler Compensation monitoring

Date start	**Year**	**Date stop**	**Year**	**Reason**
26th September	1996	27th September	1996	Missing on-board Doppler coefficient (after cal. DC converter test period)
6th June	1998	7th June	1998	No Yaw Steering Mode (after depointing anomaly)
2nd December	1998	3rd December	1998	Missing on-board Doppler coefficients (after AMI anomaly number 228)
16th February	2000	17th February	2000	Fine Pointing Mode (FPM) (due to AOCS mono-gyro qualification period)
14th April	2000	14th April	2000	Fine Pointing Mode (FPM)
5th July	2000	5th July	2000	Fine Pointing Mode (FPM) after instrument switch-on
27th September	2000	27th September	2000	Fine Pointing Mode (FPM) to upload AOCS software patch
2nd November	2000	2nd November	2000	Fine Pointing Mode (FPM)
5th December	2000	6th December	2000	Fine Pointing Mode (FPM) due to orbital manoeuvre
6th February	2001	30th March	2001	Extra Backup Mode (EBM) coarse attitude control
30th March	2001	17th June	2001	ZGM-EBM coarse attitude control
17th June	2001	21st August	2003	ZGM phase. Error in yaw angle not corrected in the ground segment processor. Data shall be reprocessed with ESACA.
24th March	2004	24th March	2004	Fine Pointing Mode (FPM) due to orbital manoeuvre
25th October	2004	27th October	2004	Series of orbital manoeuvres (OCM and FPM)
10th November	2004	11th November	2004	Intense geomagnetic storm

8th March	2005	8th March	2005	orbital manoeuvre (OCM)
11th March	2005	11th March	2005	orbital manoeuvre (FPM)
2nd November	2005	2nd November	2005	orbital manoeuvre (OCM)
1st March	2006	1st March	2006	orbital manoeuvre (OCM)
3rd November	2006	3rd November	2006	orbital manoeuvre (OCM) at 10:07:46
4th November	2006	4th November	2006	orbital manoeuvre (FCM) at 02:56:53 and 04:37:38
8th December	2006	9th December	2006	Missing on-board Doppler coefficients after AMI anomaly from 10:43 p.m. to 9th December 2006 07:18 a.m.
19th December	2006	19th December	2006	orbital manoeuvre (FCM) at 23:06:12
1st February	2007	1st February	2007	orbital manoeuvre (FCM) at 02:53:31
13th February	2007	13th February	2007	orbital manoeuvre (FCM) at 05:00:15 and 06:40:51
14th February	2007	14th February	2007	orbital manoeuvre (OCM) at 09:30:29
26th April	2007	26th April	2007	Orbital manoeuvre (FCM) at 03:12:03
11th May	2007	11th May	2007	Orbital manoeuvre (FCM) at 02:04:10
13th June	2007	13th June	2007	Orbital manoeuvre (FCM) at 03:41:38
10th September	2007	10th September	2007	Orbital manoeuvre (FCM) at 02:10:29 and 03:51:05
11th September	2007	11th September	2007	Orbital manoeuvre (FCM) at 10:01:58
12th September	2007	12th September	2007	Orbital manoeuvre (FCM) at 02:47:55 and 04:28:31
13th September	2007	13th September	2007	Orbital manoeuvre (FCM) at 05:37:30 and 07:18:16
14th September	2007	14th September	2007	Orbital manoeuvre (OCM) at 10:07:42
15th September	2007	15th September	2007	Orbital manoeuvre (FCM) at 23:00:51
16th September	2007	16th September	2007	Orbital manoeuvre (FCM) at 00:41:27
18th October	2007	18th October	2007	Orbital manoeuvre (FCM) at 02:00:00
30th October	2007	30th October	2007	Orbital manoeuvre (FCM) at 02:03:10
16th November	2007	16th November	2007	Orbital manoeuvre (FCM) at 02:51:08
4th December	2007	4th December	2007	Orbital manoeuvre (FCM) at 02:39:54
4th December	2007	4th December	2007	Orbital manoeuvre (FCM) at 04:20:30
7th December	2007	7th December	2007	Orbital manoeuvre (FCM) at 16:10:00
19th December	2007	19th December	2007	Orbital manoeuvre (FCM) at 01:28:00
10th January	2008	10th January	2007	Orbital manoeuvre (FCM) at 02:00:00
31st January	2008	31st January	2008	Orbital manoeuvre (FCM) at 03:30:45
14th February	2008	14th February	2008	Orbital manoeuvre (FCM) at 02:58:12
7th March	2008	7th March	2008	Orbital manoeuvre (FCM) at 03:00:00
20th March	2008	20th March	2008	Orbital manoeuvre (FCM) at 02:58:21
30th May	2008	30th May	2008	Orbital manoeuvre (FCM) at 01:45:00
30th May	2008	30th May	2008	Orbital manoeuvre (FCM) at 02:35:14

08th August	2008	08th August	2008	Orbital manoeuvre (FCM) at 03:16:09
2nd October	2008	2nd October	2008	Orbital manoeuvre (FCM) at 02:44:33
22nd October	2008	22nd October	2008	Orbital manoeuvre (FCM) at 16:54:26 and 18:35:02
23rd October	2008	23rd October	2008	Orbital manoeuvre (FCM) at 09:40:25
26th October	2008	26th October	2008	Orbital manoeuvre (FCM) at 20:51:22 and 21:41:36
21st November	2008	21st November	2008	Orbital manoeuvre (FCM) at 11:09:34 and 12:50:10
22nd November	2008	22nd November	2008	Orbital manoeuvre (OCM) at 10:37:59
23rd November	2008	23rd November	2008	Orbital manoeuvre (FCM) at 18:05:40 and 19:45:40
19th December	2008	19th December	2008	Orbital manoeuvre (OCM) at 03:43:00
24th January	2009	24th January	2009	Orbital manoeuvre (FCM) at 10:58:34 and 12:39:10
25th January	2009	25th January	2009	Orbital manoeuvre (OCM) at 10:27:00
29th January	2009	29th January	2009	Orbital manoeuvre (FCM) at 10:15:26
19th February	2009	19th February	2009	Orbital manoeuvre (FCM) at 02:38:37
24th March	2009	24th March	2009	Orbital manoeuvre (FCM) at 02:48:57
21st April	2009	21st April	2009	Orbital manoeuvre (FCM) at 01:54:00
30th June	2009	30th June	2009	Orbital manoeuvre (FCM) at 02:41:38
10th September	2009	10th September	2009	Orbital manoeuvre (FCM) at 02:30:00
30th September	2009	30th September	2009	Orbital manoeuvre (FCM) at 02:06:26
9th December	2009	9th December	2009	Orbital manoeuvre (INP FCM) at 10:33:34
11th December	2009	11th December	2009	Orbital manoeuvre (OCM) at 02:00:45
23rd February	2010	23rd February	2010	Orbital manoeuvre (FCM) at 00:38:07
5th March	2010	5th March	2010	Orbital manoeuvre (FCM) at 21:13:02
7th March	2010	7th March	2010	Orbital manoeuvre (FCM) at 20:08:08
15th March	2010	15th March	2010	Orbital manoeuvre (FCM) at 06:24:42 and 08:05:18
18th March	2010	18th March	2010	Orbital manoeuvre (FCM) at 21:44:22
21st March	2010	21st March	2010	Orbital manoeuvre (FCM) at 10:00:00 and 11:40:35
4th April	2010	4th April	2010	Orbital manoeuvre (FCM) at 14:15:00 and 15:55:36
17th April	2010	17th April	2010	Orbital manoeuvre (FCM) at 02:55:54
05th May	2010	05th May	2010	Orbital manoeuvre (FCM) at 23:37:16
06th May	2010	06th May	2010	Orbital manoeuvre (FCM) at 01:17:52
07th May	2010	07th May	2010	Orbital manoeuvre (OCM) at 10:49:49
09th May	2010	09th May	2010	Orbital manoeuvre (FCM) at 04:44:48 and 06:25:24
10th May	2010	10th May	2010	Orbital manoeuvre (OCM) at 10:55:37
12th May	2010	12th May	2010	Orbital manoeuvre (FCM) at 04:50:30
3rd July	2010	3rd July	2010	Orbital manoeuvre (FCM) at 00:55:03 on 02:35:39
4th July	2010	4th July	2010	Orbital manoeuvre (FCM) at 10:27:06

5th July	2010	5th July	2010	Orbital manoeuvre (FCM) at 04:53:42
5th July	2010	5th July	2010	Orbital manoeuvre (FCM) at 06:34:18
9th July	2010	9th July	2010	Orbital manoeuvre (FCM) at 01:34:28
30th July	2010	30th July	2010	Orbital manoeuvre (FCM) at 02:50:42
25th August	2010	25th August	2010	Orbital manoeuvre (FCM) at 05:32:58
17th September	2010	17th September	2010	Orbital manoeuvre (FCM) at 03:09:36
22th September	2010	22th September	2010	Orbital manoeuvre (FCM) at 11:28:19 and 13:08:55
14th October	2010	14th October	2010	Orbital manoeuvre (FCM) at 01:55:40
29th October	2010	29th October	2010	Orbital manoeuvre (FCM) at 02:13:42
26th November	2010	26th November	2010	Orbital manoeuvre (FCM) at 03:02:08
7th January	2011	7th January	2011	Orbital manoeuvre (FCM) at 02:06:27

The Doppler compensation evolution for cycle 164 is showed in Figure 6. The monitoring shows a daily average of the CoG of the compensated received signal around 60 Hz and -10 Hz for the Fore and Aft antenna respectively. For the Mid antenna it was around 240 Hz. The standard deviation of the CoG was around 1500 Hz for the Fore and Aft antenna and around 2700 Hz for the Mid antenna.

ERS-2 WindScatterometer: DOPPLER COMPENSATION Evolution (UWI)

Least-square poly. fit fore beam	Center of gravity = 11.184 +(0.0036)*day	Standard Deviation = 5083.5 +(-0.780)*day
Least-square poly. fit mid beam	Center of gravity = -605.5 +(0.1918)*day	Standard Deviation = 5750.9 +(-0.658)*day
Least-square poly. fit aft beam	Center of gravity = -234.4 +(0.0532)*day	Standard Deviation = 5218.4 +(-0.808)*day

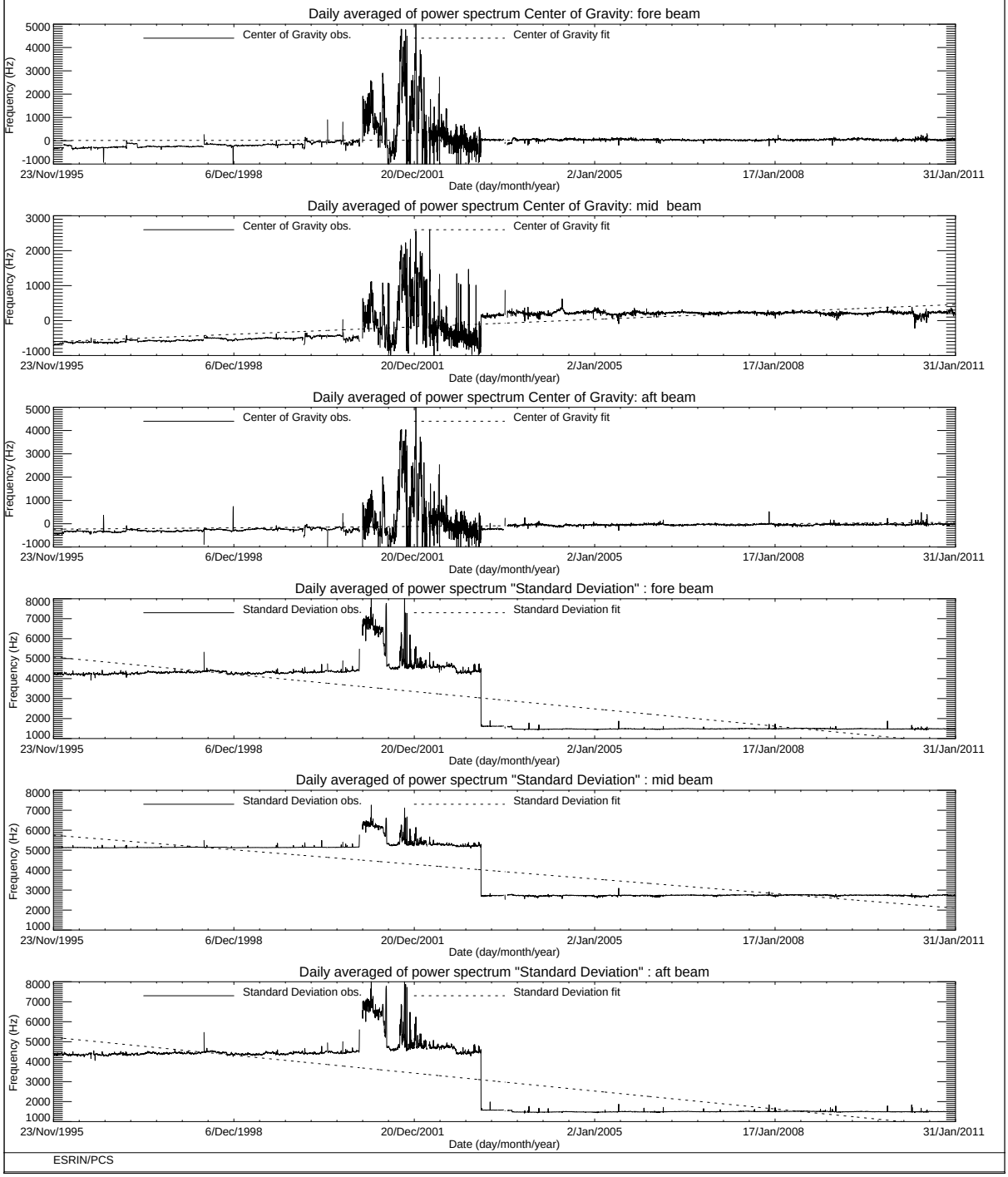

FIGURE 5 ERS-2 Scatterometer: Centre of Gravity and standard deviation of received power spectrum since the beginning of the mission.

ERS-2 WindScatterometer: DOPPLER COMPENSATION Evolution (UWI)

Least-square poly. fit fore beam	Center of gravity = 62.870 +(-0.083)*day	Standard Deviation = 1482.2 +(-0.066)*day
Least-square poly. fit mid beam	Center of gravity = 242.91 +(-0.375)*day	Standard Deviation = 2721.5 +(0.1914)*day
Least-square poly. fit aft beam	Center of gravity = -13.19 +(-0.364)*day	Standard Deviation = 1489.6 +(0.1350)*day

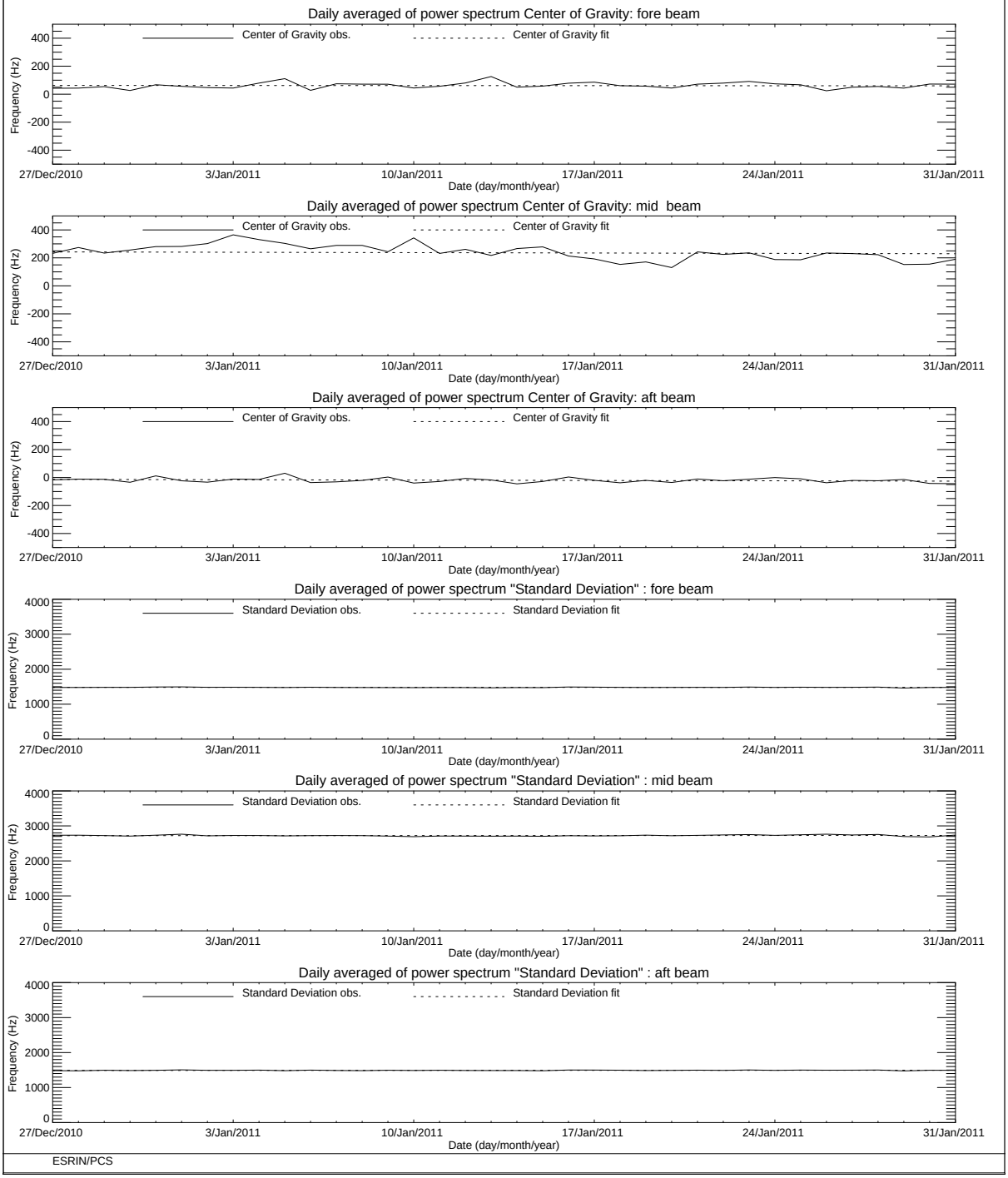

FIGURE 6 ERS-2 Scatterometer: Centre of Gravity and standard deviation of received power spectrum for cycle 164.

3.2 Noise power level I and Q channel

The results of the monitoring are shown in Figure 7 (long-term) and Figure 8 (cycle 164). The first set of three plots presents the noise power evolution for the I channel while the second set shows the Q channel. From the plots one can see that the noise level is more stable in the I channel than in the Q one. The I and Q receivers are inside the same box and any external interference should affect both channel. The fact that the Q receivers are closer to the ATSR-GOME electronics could have some impact, but there is no clear explanation on that behavior. From 5th December 1997 until November 1998 some high peaks appear in the plots. These high values for the daily mean are due to the presence for these special days of a single UWI product with an unrealistic value in the noise power field of its Specific Product Header. The analysis of the raw data used to generate these products lead in all cases to the presence of one source packet with a corrupted value in the noise field stored into the source packet Secondary Header. The reason why noise field corruption is beginning from 5th December 1997 and last until November 1998 is at present unknown. It is interesting to note that at the beginning of December 1997, we started to get as well the corruption of the Satellite Binary Times (SBTs) stored in the EWIC product. The impact in the fast delivery products was the production of blank products starting from the corrupted EWIC until the end of the scheduled stop time. A change in the ground station processing in March 1998 overcame this problem.

Since 9th August 1998 until March 2000 some periods with a clear small instability in the noise power have been recognized, Table 3 gives the detailed list.

TABLE 3 ERS-2 Periods with instability in the noise power

Start date	Stop date	Year
9th August	26th October	1998
29th November	6th December	1998
23rd December	24th December	1998
7th June	10th June	1999
17th August	22nd August	1999
8th September	9th September	1999
3rd October	8th October	1999
16th October	18th October	1999
26th October	28th October	1999
25th December	2nd January	2000
10th February	11th February	2000
19th March	26th March	2000

To better understand the instability of the noise power the PCS has carried out investigations in the Scatterometer raw data (EWIC) to compute the noise power with more resolution. The result is that for the orbits affected by the instability the noise power had a decrease of roughly 0.7 dB for the fore and aft signals and a decrease of roughly 0.6 dB in the mid beam case (see the report for the cycle 42). The decrease of the noise power during the orbits affected by the instability is comparable with the decrease of the internal calibration level that occurred during the same orbits. The reason of this instability (linked to the AMI anomalies) is still unknown. On 28th February 2003 the Scatterometer receiver gain has been increased by 3 dB to optimize the usage of the on-board ADC converter. This explains the increase of the noise for the Fore and Aft beam channel. For the mid beam channel the noise still remains not measurable.

On 17th February 2006 a high peak was detected in the noise power, causing the daily average for that day very high. The case has been deeply investigated and a technical note (Ref OSME-DPQC-SEDA-TN-06-0163) is available. The cause was an acquisition problem that corrupted one source packet and not an instrument anomaly. The same happened on April 24th 2006 (cycle 115).

On 8th September 2006 a high peak in the noise power of the Mid beam has been detected. The event occurred between 17:41:54 and 17:42:43 (UTC) and the noise power reached the value of 43 ADC (fore beam) and 19 ADC (mid beam). Those values had affected the daily average and are clear present in the plots of the Figure 7. That anomaly has been deeply investigated in the Technical Note OSME-DPQC-SEDA-TN-06-0251 and cannot be linked to any anomaly in the acquired data. The conclusion of the investigation was that a problem had occurred in the transmitter or in the pulse generator of the AMI instrument. At that time the AMI was in wind only mode so no additional comparison with SAR data can be done. Similar peaks had been noted also for September 15th and 18th. ESOC has checked the Mission Plan and noticed that in all three events the peak in the noise power occurred very close to 6 minutes after the start of a Wind mode and 40 minutes after ascending node crossing.

The evolution of the noise power during the cycle 164 was stable. The daily average for the Fore and Aft beam noise is around 1.7 ADC (I) and around 1.6 ADC (Q), respectively. For the Mid beam the noise is around 1.2 ADC both I and Q.

ERS-2 WindScatterometer: NOISE Level Evolution (UWI)

Least-square line fit fore beam: I = 807.84 +(0.2033)*day Q = 752.98 +(0.1929)*day

I channel: No line fit standard deviation too hight Q channel: No line fit standard deviation too hight

Least-square line fit aft beam: I = 803.21 +(0.1957)*day Q channel: No line fit standard deviation too hight

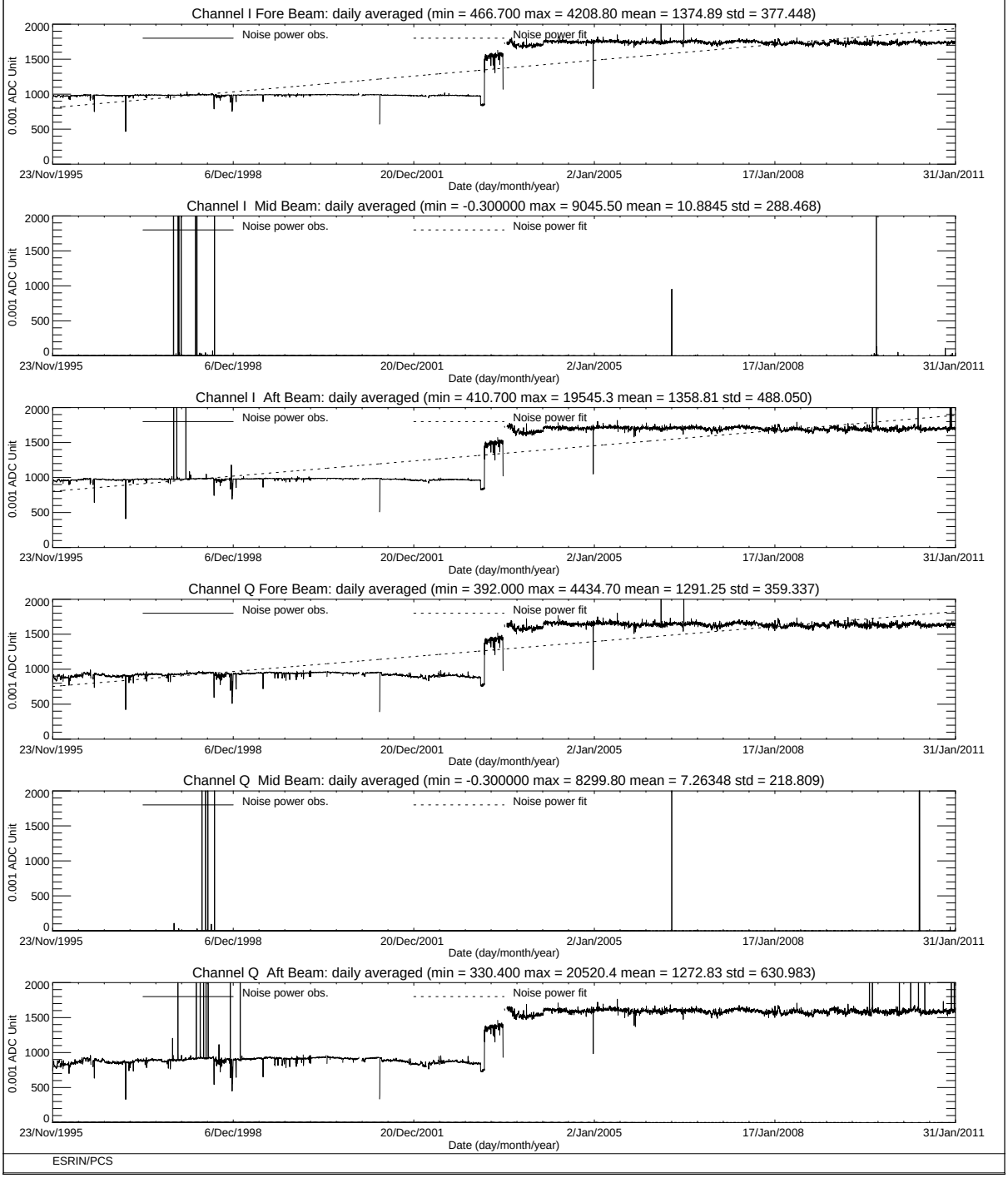

FIGURE 7 ERS-2 Scatterometer: noise power I and Q channel since the beginning of the mission.

ERS-2 WindScatterometer: NOISE Level Evolution (UWI)

Least-square line fit fore beam: I = 1738.9 +(0.1390)*day Q = 1636.8 +(0.3272)*day

Least-square line fit mid beam: I = 1.2564 +(-0.039)*day Q = -0.233 +(0.0425)*day

I channel: No line fit standard deviation too hight Q channel: No line fit standard deviation too hight

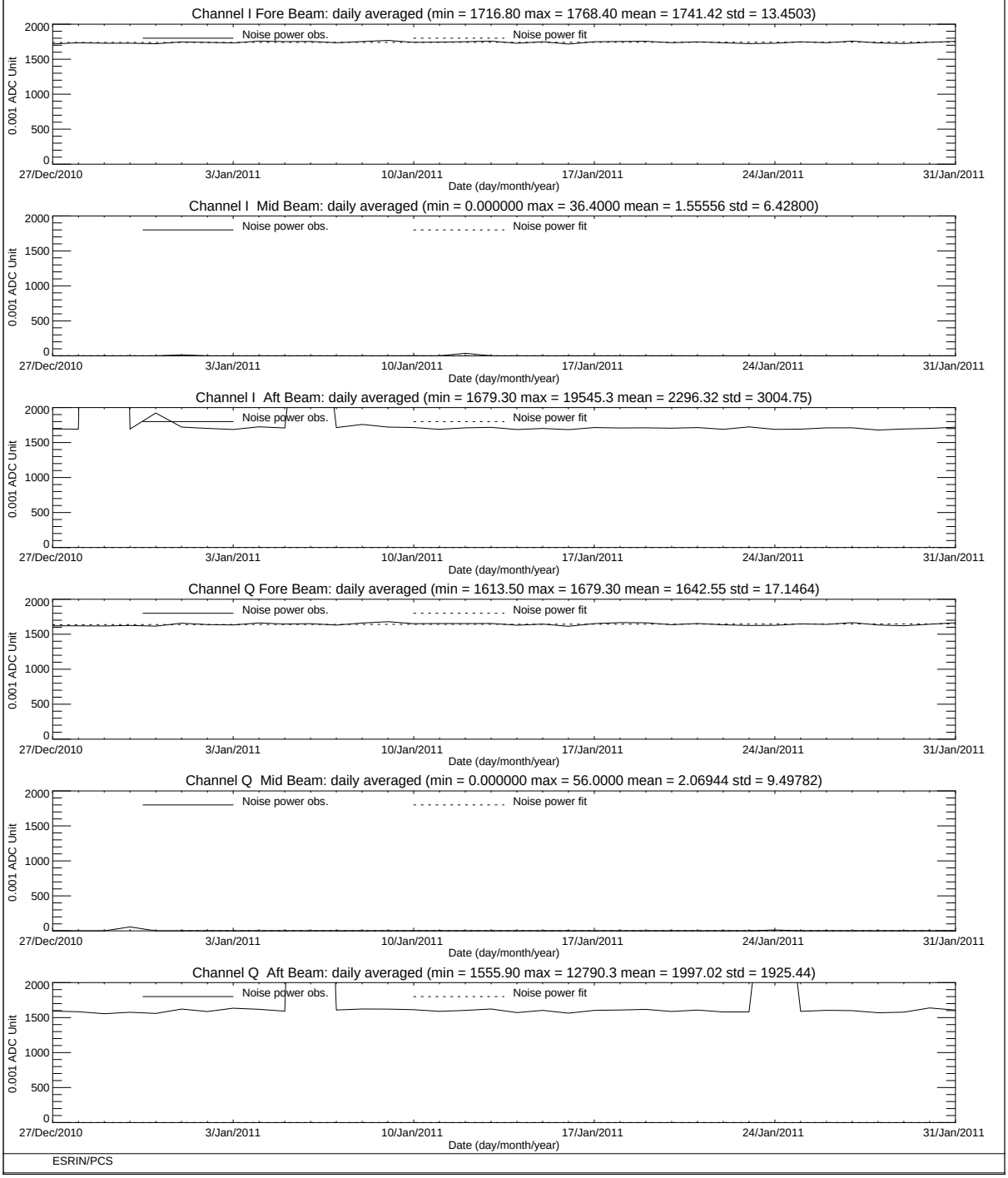

FIGURE 8 ERS-2 Scatterometer: noise power I and Q channel for cycle 164.

3.3 Power level of internal calibration pulse

For the internal calibration level, the results are shown in Figure 9 (long-term) and Figure 10 (cycle 164). The high value of the variance in the fore beam until August, 12th 1996 is due to the ground processing. In fact all the blank source packets ingested by the processor were recognized as Fore beam source packets with a default value for the internal calibration level. The default value was applicable for ERS-1 and therefore was not appropriate for ERS-2 data processing. On August 12th, 1996 a change in the ground processing LUT overcame the problem. Since the beginning of the mission a power decrease is detected. The power decrease is regular and affects the AMI when it is working in wind-only mode, wind/wave mode and image mode indifferently. The average power decrease is around 0.08 dB per cycle (0.0022 dB/day) and is clearer after August, 6th 1996 when the calibration subsystem has been changed. The reason of the power decrease is because the TWT is not working in saturation, so that a variation in the input signal is visible in the output. The variability of the input signal can be two-fold: the evolution of the pulse generator or the tendency of the switches between the pulse generator and the TWT to reset themselves into a nominal position. These switches were set into an intermediate position in order to put into operation the Scatterometer instrument (on 16th November 1995). To compensate for this decrease, on 26th October 1998 (cycle 37) 2.0 dB were added to the Scatterometer transmitted power and on 4th September 2002 (cycle 77) were added 3.0 dB. On 28th February 2003 (cycle 82) the Scatterometer receiver gain was increased by 3 dB to improve the usage of the on-board ADC converter. These events are clearly displayed by the large steps show in Figure 9.
Since 9th August 1998 until March 2000 the internal calibration level shows instability after an AMI or platform anomaly (see reports from cycle 35 to cycle 52). This instability is very well correlated with the fluctuations observed in the noise power. On 13th July 2000 a high peak (+3.5 dB) was detected in the transmitted power. This event has been investigated deeply by PCS and ESOC. The results of the analysis are reported in the technical note “ERS-2 Scatterometer: high peak in the calibration level” available in the PCS. The high transmitted power was detected after an arcing event which occurred inside the HPA. After that event the transmitted power had an average increase of roughly 0.14 dB.

During the cycle 164 the mean transmitted power evolution had a mean decreasing trend of 0.03 dB. This value is lower than the nominal decreasing trend of 0.1 dB/Cycle detected since the beginning of the mission.

ERS-2 WindScatterometer: Internal CALIBRATION Level Evolution (UWI)

Least-square polynomial fit fore beam	gain (dB) per day 0.0000	1044.72 +(0.00377946)*day
Least-square polynomial fit mid beam	gain (dB) per day 0.0000	309.850 +(0.000634208)*day
Least-square polynomial fit aft beam	gain (dB) per day 0.0000	1033.35 +(0.00454725)*day

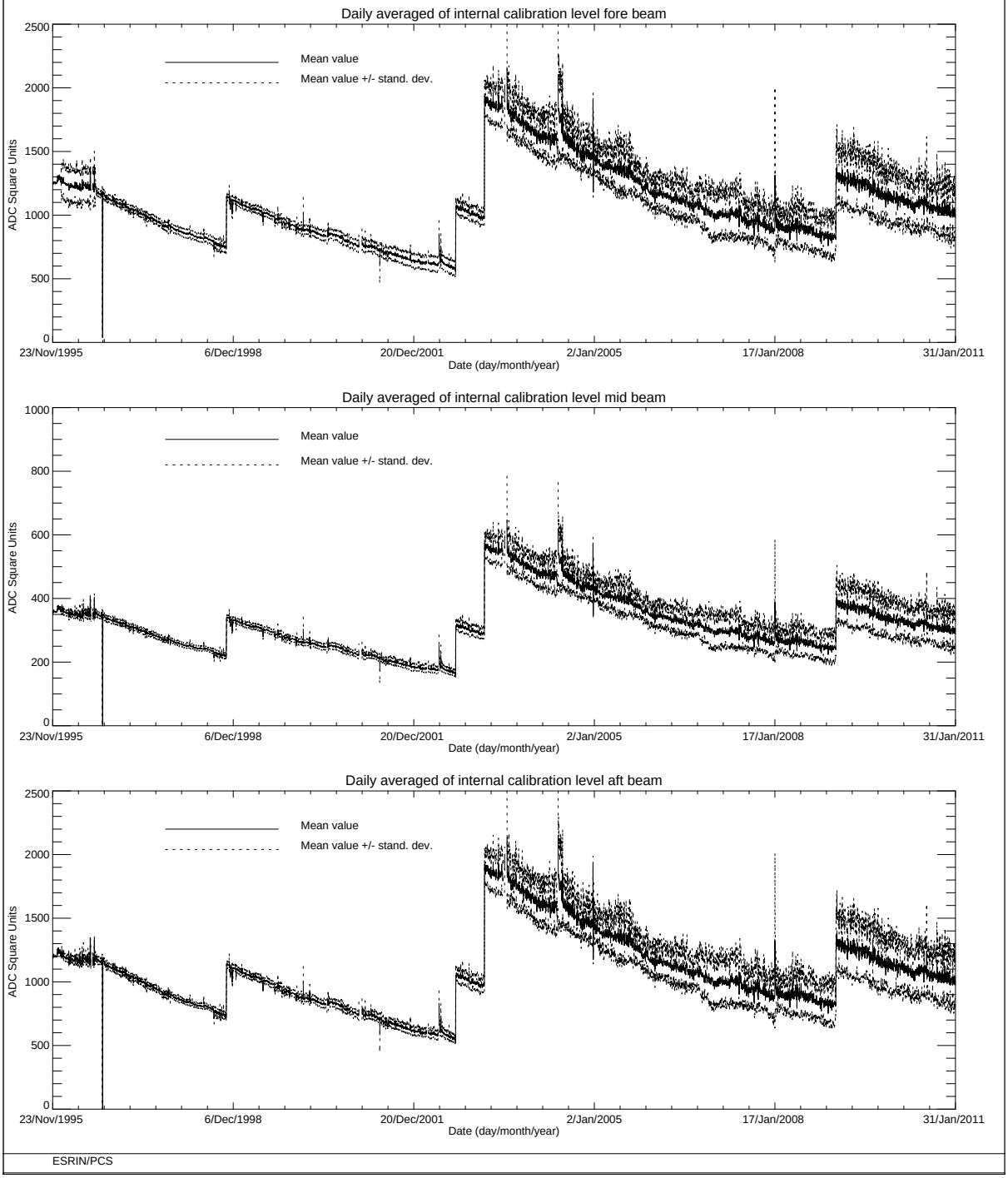

FIGURE 9 ERS-2 Scatterometer: power of internal calibration pulse since the beginning of the mission.

ERS-2 WindScatterometer: Internal CALIBRATION Level Evolution (UWI)

Least-square polynomial fit fore beam	gain (dB) per day -0.0010	1018.62 +(-0.233819)*day
Least-square polynomial fit mid beam	gain (dB) per day -0.0009	298.882 +(-0.0584375)*day
Least-square polynomial fit aft beam	gain (dB) per day -0.0007	1012.14 +(-0.152472)*day

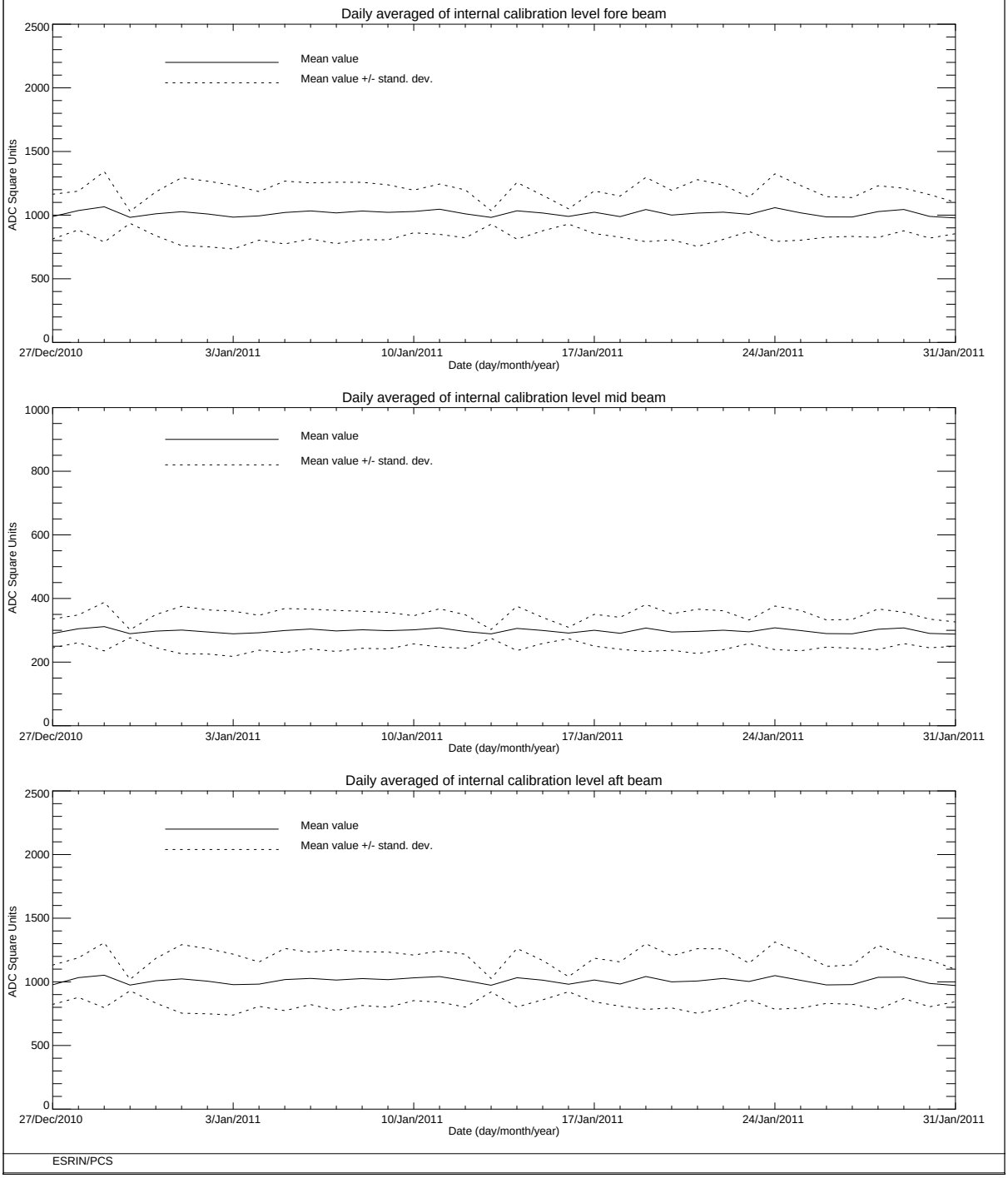

FIGURE 10 ERS-2 Scatterometer: power of internal calibration level cycle 164.

4 Products performance

The PCS carries out a quality control of the winds generated from the WSCATT data. External contributions to this quality control (from ECMWF) are also reported in this chapter.

4.1 Products availability

One of the most important points in the monitoring of the products performance is their availability. The Scatterometer is a part of ERS payload and it is combined with a Synthetic Aperture Radar (SAR) into a single Active Microwave Instrument (AMI). The SAR users requirements and the constraints imposed by the on-board hardware (e.g. amount of data that can be recorded in the on-board tape) set rules in the mission operation plan.

The principal rules that affected the Scatterometer instrument data coverage are:
• Over the Ocean the AMI is in wind/wave mode (Scatterometer with small SAR imagettes acquired every 30 sec.) and the ATSR-2 is in low rate data mode.
• Over the Land the AMI is in wind only mode (only Scatterometer) and the ATSR-2 is in high rate mode. (Due to on board recorder capacity, ATSR-2 in high rate is not compatible with SAR wave imagettes acquisitions.) This strategy preserves the Ocean mission.
• The SAR images are planned as consequence of users' request.
Moreover:

- since July 16th 2003 the ERS-2 Low Rate mission is continued within only the visibility of ESA ground stations over Europe, North Atlantic, the Arctic and western North America. The reason was the failure of both on-board tape recorders.
- During the cycles 64 – 92 (June 2001 since 25th February 2004) the AMI instrument was operated in wind/wave mode also over the land. The reason was because the SAR wave data was used to estimate the satellite mispointing along the full orbit. Since 25th February onwards the nominal mission scenario has been resumed, with the AMI instrument in wind only mode over the land (and consequently ATSR was operated again in High Rate over land). The mispointing performances (in particular the yaw error angle) along the full orbit are computing by analyzing the Scatterometer data.

In order to maximize the data coverage, after the on-board tape recorder failure, an upgrade of the ERS ground segment acquisition scenario has been performed.
In that framework the following has been implemented:

- Since September 7th 2003 the ground station in Maspalomas, Gatineau and Prince Albert are acquiring and processing data for all the ERS-2 satellite passes within the station visibility (apart from passes for which other satellites have an higher priority).
- To further increase the wind coverage of the North Atlantic area, since December 8th,

2003 is operative a new ground Station in West Freugh (UK) and data from this new station are available to the user since mid January 2004. Due to its location, the West Freugh acquisitions have some overlap with those from three other ESA stations, Kiruna, Gatineau or Maspalomas. The station overlap depends on the relative orbit of the satellite. Consequentially, overlapping wind Scatterometer LBR data may be included in two products. Since the two products are generated at different ground stations the overlap may not be completely precise, with a displacement up to 12 Km and slight differences in the wind data itself.

- Since March, 3rd 2004, Matera station is acquiring and processing low rate bit data for all the passes for which is planned a SAR acquisition. This means for the Scatterometer data coverage a limited improvement due to the fact that is acquired only a passage with some planned SAR activity.
- Since February 2005 a new acquisition station in Miami (US) is in operations. This new station allows a full data coverage of the Gulf of Mexico and part of the Pacific Ocean on the west Mexico coast.
- Since 25th, June 2005 a new acquisition stations have been put into operations in Beijing. It covers part of China and Oriental Asia.
- Since 5th July 2005 McMurdo ground station is operational in the South Pole. It covers all the Antarctic region.
- Since 5th December 2005 the Hobart station is operational and it is covering the Australian and New Zealand area. Hobart data has been disseminated into BUFR format since February 13th 2006.
- At the end of August 2006 a new ground station in Singapore has been installed and products are distributed to the users since October 19th 2006.
- At the end of September 2007 a new ground station has been put into operation in Chetumal (Mexico). Products are distributed to the users since October 18th 2007.
- On May 2008 a new ground station is operational in Johannesburg. Data has been disseminated to users since July 2008.

Figure 11 shows the AMI operational modes for cycle 164. Each segment of the orbit has different color depending on the instrument mode: brown for wind only mode, blue for wind-wave mode and green for image mode. The red and yellow colors correspond to gap modes (no data acquired). For cycle 164 the percentage of the ERS-2 AMI activity is shown in table 4. The values for cycle 164 show a slight decrease of SAR activity for ascending passes (2.89%, was 3.19%) and an increase for descending passes with respect to the cycle 163 (24.21%, was 19.35%).

TABLE 4 ERS-2 AMI activity (cycle 164)

Ami Mode	Ascending passes	Descending passes
Wind and Wind-Wave	**91.97 %**	**72.26 %**
Image	**2.89 %**	**24.21 %**
Gap and others	**5.11 %**	**6.42 %**

Table 5 reports the major data lost (day or more) due to the test periods, AMI and satellite anomalies or ground segment anomalies occurred after 6th August, 1996 (before that day for many times data were not acquired due to the DC converter failure).

TABLE 5 ERS-2 Scatterometer mission major data lost (day or more) after 6th, August 1996

Start date	Stop Date	Reason
September 23rd, 1996	September 26th , 1996	ERS 2 switched off due to a test period
February 14th , 1997	February 15th , 1997	ERS 2 switched off due to a depointing anomaly
June 3rd, 1998	June 6th, 1998	ERS 2 switched off due to a depointing anomaly
November 17th , 1998	November 18th , 1998	ERS 2 switched off to face out Leonide meteor storm
September 22nd 1999	September 23rd 1999	ERS 2 switched off due to Year 2000 certification test
November 17th , 1999	November 18th , 1999	ERS 2 switched off to face out Leonide meteor storm
December 31st ,1999	January 2nd , 2000	ERS 2 switched off Y2K transition operation
February 7th ,2000	February 9th , 2000	ERS 2 switched off due to new AOCS s/w up link
June 30th , 2000	July 5th , 2000	ERS 2 Payload switched off after RA anomaly
July 10th , 2000	July 11th , 2000	ERS 2 Payload reconfiguration
October 7th , 2000	October 10th 2000	ERS 2 Payload switched off after AOCS anomaly
January 17th , 2001	February 5th , 2001	ERS 2 Payload switched off due to AOCS anomaly
May 22nd , 2001	May 24th , 2001	ERS 2 Payload switched off due to platform anomaly
May 25th , 2001	May 25th , 2001	AMI switched off due thermal analysis
November 17th , 2001	November 18th , 2001	ERS 2 switched off to face out Leonide meteor storm
November 27th , 2001	November 28th , 2001	ERS 2 payload off due to 1Gyro Coarse Mode commissioning
March 8th , 2002	March 20th , 2002	ERS 2 payload unavailability after RA anomaly
May 19th ,2002	May 24th 2002	AMI switched off due to arc events
May 24th , 2002	May 28th , 2002	AMI partially switched off due to arc events
May 31st 2002	June 3rd 2002	Gatineau orbits partially acquired due to antenna problem
June 4th , 2002	June 5th , 2002	AMI partially switched-off due to arc events
July 25th , 2002	July 25th , 2002	AMI switched off HPA voltage too low
September 11th , 2002	September 11th , 2002	AMI switched off macrocommand transfer error
November 17th, 2002	November 18th, 2002	ERS-2 switched off to face out Leonide meteor storm
December 9th , 2002	December 10th , 2002	IDHT anomaly no data recorded on board

December 20th , 2002	December 20th 2002	IDHT anomaly no data recorded on board
January 14th , 2003	January 14th, 2003	IDHT anomaly no data recorded on board
May 6th , 2003	May 19th , 2003	AMI off due to bus reconfiguration
June 22nd , 2003	July 16th ,2003	IDHT recorders test no data acquired
Since July 16th ,2003		Regional Mission Scenario. Data available only within the visibility of ESA ground station
May 21st, 2004	May 25th, 2004	AMI in refuse mode due to excessive HPA arcing
June 22nd ,2004	June 22nd , 2004	AMI in refuse mode due to excessive HPA arcing
September 23rd, 2004	September 24th, 2004	AMI switched down
December 16th, 2004	December 17th, 2004	AMI memory test
December 26th, 2004	December 26th, 2004	IDHT anomaly. No data acquired
December 27th, 2004	December 28th, 2004	Payload off due to on board anomaly
January 23rd , 2005	January 23rd , 2005	AMI switched down (00.51 a.m. – 1.26 p.m.)
February 26th , 2005	February 26th , 2005	AMI switched down (01.20 a.m. – 12.37 a.m.)
May 23rd , 2005	May 24th , 2005	ERS 2 payload unavailability after RA anomaly
Jun 20th, 2005	Jun 21st, 2005	AMI switched off caused by RBI status error (08:44 p.m. – 10:13 a.m.)
December 8th, 2006	December 8th, 2006	AMI switched down to Standby/MCMD Execution Inhibited due to Format Acquisition Error (02:04 p.m. – 10:43 p.m.)
April, 13th, 2007	April 13th, 2007	AMI Switched down to Standby/MCMD Execution Inhibited due to Format Acquisition Error (03:10 a.m. – 12.06 p.m.)
May, 22nd, 2007	May, 22nd, 2007	AMI Switched down to Standby/MCMD Execution Inhibited due to Acquisition Errors (01:50 p.m. – 07.04 p.m.)
June, 10th, 2007	June, 10th, 2007	AMI Switched down to Standby/MCMD Execution Inhibited due to Format Length and ICU Begin Identifier Errors (00:55 a.m. – 10.13 a.m.)
June, 11th, 2007	June, 12th, 2007	AMI Switched down to Standby/MCMD Execution Inhibited due to Emergency Switchdown requested by AMI ICU (10:39 p.m. – 10.49 a.m.)
July, 27th, 2007	July, 27th, 2007	AMI switchdown to Standby/MCMD Execution Inhibited due to RBI Status Error (00:44 a.m. - 09:43 a.m).
January, 17th, 2008	January, 17th, 2008	AMI switched down to Heater/MCMD Refuse mode due to HPA Arcing (04:01 a.m. – 07:22 p.m.)
January, 17th, 2008	January, 18th, 2008	AMI switched down to Heater/MCMD Refuse mode due to HPA Arcing (07:51 p.m. – 12:49 p.m.)
January, 18th, 2008	January, 18th, 2008	AMI switched down to Heater/MCMD Refuse mode due to HPA Arcing (03:26 p.m. – 03:39 p.m.)
January, 18th, 2008	January, 18th, 2008	AMI switched down to Heater/MCMD Refuse mode due to HPA Arcing (08:12 p.m. – 08:31 p.m.)
January, 18th, 2008	January, 19th, 2008	AMI switched down to Heater/MCMD Refuse mode due to HPA Arcing (10:37 p.m. – 01:32 a.m.)
January, 20th, 2008	January, 20th, 2008	AMI switched down to Heater/MCMD Refuse mode due to HPA Arcing (02:04 a.m. – 07:53 a.m.)
February, 5th, 2007	February, 5th, 2007	AMI switched down to Standby/MCMD Execution Inhibited due to Format Length and ICU Begin Identifier Errors (02:05:09 a.m. – 05:43:33 p.m.)
February, 6th, 2007	February, 6th, 2007	AMI switched down to Standby/MCMD Execution Inhibited due to Format Length and ICU Begin Identifier Errors (12:14:23 p.m. – 12:52:51 p.m.)
April, 14th, 2008	April, 14th, April	AMI switched down to Standby/MCMD Execution Inhibited due to Format Length and ICU Begin Identifier Errors (13:43:34 – 18:57:19)

April, 30th, 2008	April, 30th, 2008	AMI switched down to Standby/MCMD Refuse Mode due to 228 ICU Req. (08:25:42 – 11:44:05)
June, 12th, 2008	June, 12th, 2008	AMI switched down to Heater/MCMD Refuse Mode due to incorrect timetag entered for quarterly AMI Science Data Memory Test (08:44:43 – 09:10:34)
June, 16th, 2008	June, 12th, 2008	AMI Switched down to Standby/MCMD Execution Inhibited due to Format Length and ICU Begin Identifier Errors (01:17:26 – 10:24:10).
June, 20th, 2008	June, 20th, 2008	AMI Emergency Switchdown to Standby/MCMD Execution Inhibited due to RBI Status Error (13:12:22 – 18:20:40).
June, 29th, 2008	June, 29th, 2008	AMI unavailable for PL Synchronisation (20:23:00 – 20:48:59)
July, 26th, 2008	July, 26th, 2008	AMI in Standby/MCMD Refused due to Anomaly 228 ICU REQ 1500 0082 (18:38:30 – 22:40:52)
August, 31st, 2008	September, 1st, 2008	AMI switchdown to Standby/MCMD Execution Inhibited due to Format Length and ICU Begin Identifier Errors (22:10:15 – 12:15:06)
November, 14th, 2008	November, 14th, 2008	AMI Emergency Switchdown to Standby/MCMD Execution Inhibited due to RBI Status Error (13:19:02 – 19:39:49)
January, 27th, 2009	January, 27th, 2009	AMI unavailable due to Upconverter Gain Update for Wind Mode (09:02:12 – 09:28:00).
February, 4th, 2009	February, 4th, 2009	AMI unavailable due to Upconverter Gain Update for Wave Mode (13:09:51 – 13:31:00).
February, 9th, 2009	February, 9th, 2009	AMI unavailable for PL Synchronisation (11:00:36 – 11:00:46)
February, 9th, 2009	February, 9th, 2009	AMI Swithdown to Standby/MCMD Refuse Mode due to 228 ICU REQ (11:01:14 – 16:17:02)
April, 7th, 2009	April, 7th, 2009	AMI Swithdown to Standby/MCMD Refuse Mode due to 228 ICU REQ (08:18:03 – 11:25:05)
April, 11th, 2009	April, 11th, 2009	AMI switched down to Heater/MCMD Refuse mode due to HPA Arcing (10:59 – 13:42)
May, 24th, 2009	May, 24th, 2009	AMI Emergency Switchdown to Standby/MCMD Execution Inhibited due to to Format Length and ICU Begin Identifier Errors (00:50:57 – 11:47:59)
June, 1st, 2009	June, 1st, 2009	AMI Swithdown to Standby/MCMD Refuse Mode due to 228 ICU REQ (03:42:20 – 09:05:31)
August, 3rd , 2009	August, 4th , 2009	AMI Swithdown to Standby/MCMD Refuse Mode due to concurrent 216 MCD ERR and 228 ICU REQ (23:30:21 - 08:39:18)
August, 7th , 2009	August, 7th , 2009	AMI Switched to HEATER/REF due to Command Rejection (09:04:43 - 13:34:49)
August, 20th , 2009	August, 20th , 2009	AMI EQ-SOL , MCMD /REF due to Anomaly 228 ICU REQ 1500 0082 (00:01:49 - 10:17:46)
August, 24th , 2009	August, 24th , 2009	AMI Swithdown to Standby/MCMD Refuse Mode due to 228 ICU REQ (06:20:45 – 13:29:41)
September, 4th, 2009	September, 4th, 2009	AMI Swithdown to Standby/MCMD Refuse Mode due to 228 ICU REQ (09:13:17 – 14:36:19)
September, 9th , 2009	September, 10th, 2009	AMI in Heater/MCMD Refuse Mode due to End of Wind Anomaly (11:35:59 - 14:36:19)
September, 11th, 2009	September, 11th, 2009	AMI Swithdown to Standby/MCMD Refuse Mode due to 228 ICU REQ (16:09:45 – 18:32:40)
October, 10th, 2009	October, 10th, 2009	AMI Swithdown to HEATER/REF due to Command Failure (07:42:26 - 10:03:33)
October, 13th, 2009	October, 13th, 2009	AMI Swithdown to Standby/MCMD INHIBIT Mode due to 222 FMT LEN (12:40:44 – 19:07:31)
January, 14th, 2010	January, 14th, 2010	AMI Swithdown to Standby/MCMD Refuse Mode due to 228 ICU REQ (12:08:01 – 16:29:39)
January,31st, 2010	January, 31st, 2010	AMI unavailable for PL Synchronization (08:13:48 – 11:27:34)
February, 9th, 2010	February, 9th, 2010	AMI Swithdown to Standby/MCMD Execution Inhibited due to Format Length Errors and ICU Begin Identifiers Errors

		(00:29:22 – 13:06:44)
February, 28th, 2010	February, 28th, 2010	AMI unavailable for PL Synchronization (11:59:26-13:09:19) and subsequent Heater/MCMD Refuse Mode due to PL synchronization anomaly
March, 7th, 2010	March, 7th, 2010	AMI unavailable for PL Synchronization (19:25:50-19:50:04)
March, 19th, 2010	March, 19th, 2010	AMI in Heater/Refuse due to Gap mode time out (04:09:42-04:45:20)
May, 3rd , 2010	May, 3rd , 2010	AMI Switchdown to Heater/ MCMD Refused due to End of Wind Anomaly (02:04:35-07:54:56)
May, 25th , 2010	May, 26th , 2010	AMI Swithdown to Standby/MCMD Refused after anomalies 222, 224, 228 (11:10:54 – 09:19:44)
July, 16th , 2010	July, 16th , 2010	AMI in Heater/Refuse due to Gap mode time out (16:58:00 – 18:47:38)
July, 22nd , 2010	July, 22nd , 2010	AMI unavailable for PL Synchronization (20:56:14 – 22:04:07)
August, 3rd , 2010	August, 3rd , 2010	AMI Switchdown to Heater/ MCMD Refused Mode (14:45:22 - 16:14:02)
September, 29th, 2010	September 29th, 2010	AMI Switchdown to Heater / MCMD Refuse Mode (15:03:27 – 16:26:34)
October, 21st, 2010	October, 21st, 2010	AMI unavailable due to payload synchronization (18:25:22 – 18:44:20)
December, 24th, 2010	December, 25th, 2010	IDHT Switchdown to Standby / MCMD Execution Inhibited after Ano 217 MCD ERR (20:09:22 - 07:51:44)
January, 4th, 2010	January, 4th, 2010	AMI set to HEATER mode for eclipse (08:03:00 – 09:13:13)
January, 4th, 2010	January, 4th, 2010	AMI set to HEATER mode for eclipse (09:44:00 – 10:27:10)

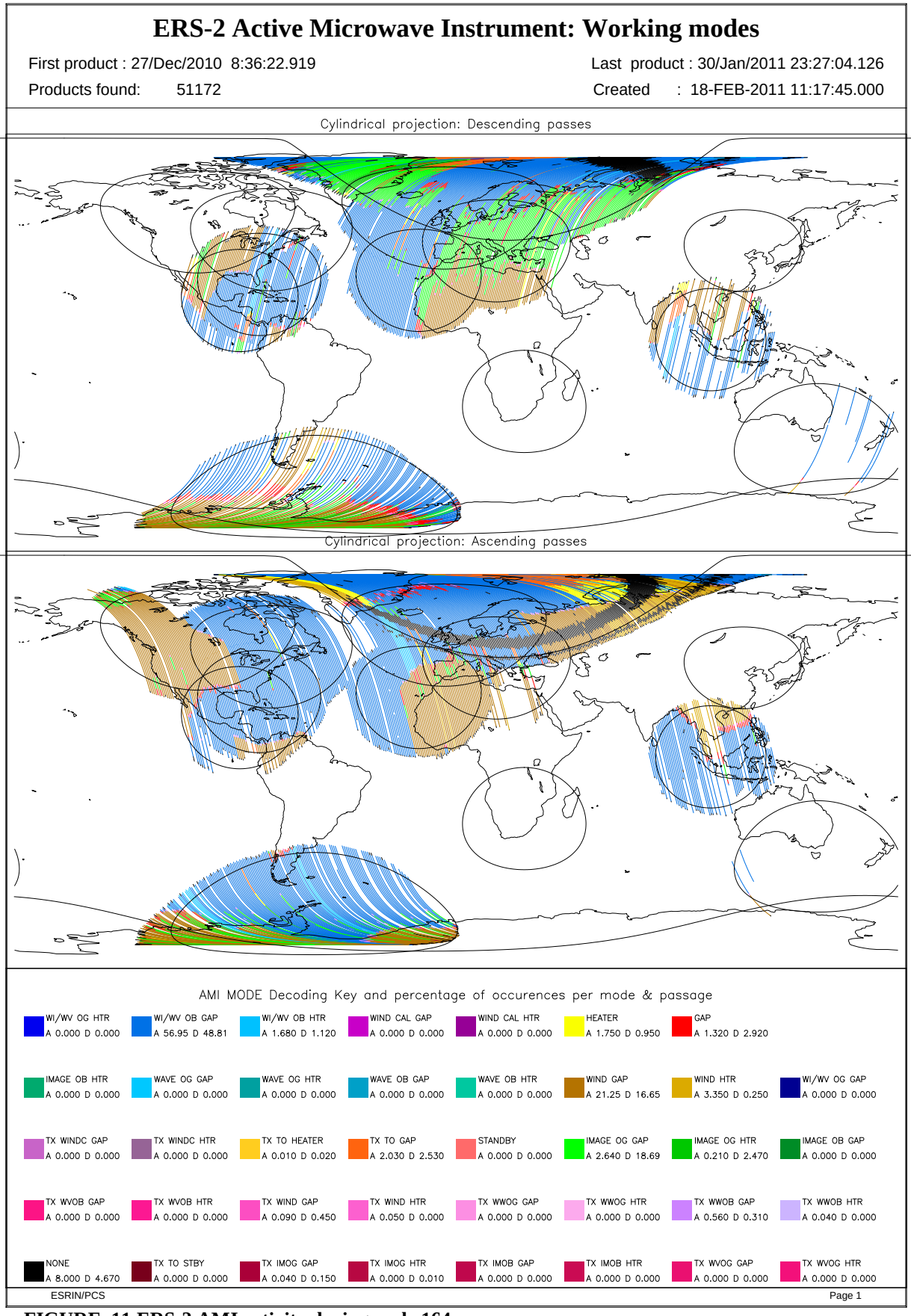

FIGURE 11 ERS-2 AMI activity during cycle 164.

4.2 PCS Geophysical Monitoring

The routine analysis is summarized in the plots of figure 12; from top to bottom:

• the monitoring of the valid sigma-nought triplets per day.
• the evolution of the wind direction quality. The ERS wind direction (for all nodes and only for those nodes where the ambiguity removal has worked properly) is compared with the ECMWF forecast. The plot shows the percentage of nodes for which the difference falls in the range -90.0, +90.0 degrees.
• the monitoring of the percentage of nodes whose ambiguity removal works successfully.
• the comparison of the wind speed deviation: (bias and standard deviation) with the ECMWF forecast.

The results since August 6th, 1996 until the beginning of the operation with the Zero Gyro Mode (ZGM) in January 2001 can be summarized as:
• High quality wind products has been distributed since Mid March 1996 (end of calibration and validation phase)
• The number of valid sigma-nought distributed per day was almost stable with a small increase after June 29th, 1999 due to the dissemination in fast delivery of the data acquired in the Prince Albert station (Canada).
• The wind direction is very accurate for roughly 93% of the nodes, the ambiguity removal processing successfully worked for more than 90.0% of the nodes.
• The UWI wind speed shows an absolute bias of roughly 0.5 m/s and a standard deviation that ranges from 2.5 m/s to 3.5 m/s with respect to the ECMWF forecast.
• The wind speed bias and its standard deviation have a seasonal pattern due to the different winds distribution between the winter and summer season.
• Two important changes affect the speed bias plot.
• the first is on June 3rd , 1996 due to the switch from ERS-1 to ERS-2 data assimilation in the meteorological model.
• the second which occurred at the beginning of September 1997, is due to the new monitoring and assimilation scheme in ECMWF algorithms (4D-Var).
• Since 19th April 1999 two set of meteo-table (meteorological forecast centred at 00:00 and 12:00 of each day) are used in the ground processing. This allowed the processing of wind data with 18 and 24 hours meteorological forecast instead of the 18, 24, 30 36 hours forecast. The comparison between data processed with the 18-24 hours forecast instead of 30-36 hours forecast shown an increase in the number of ambiguity removed nodes with a neutral impact in the daily statistics.

• The mono-gyro AOCS configuration (see report for cycle 50) that was operative from 7th February 2000 to 17th January 2001 did not affect the wind data performance.
During the Zero Gyro Mode (ZGM) phase the dissemination of the fast delivery Scatterometer data to the users has been interrupted on 17th January 2001 due to degraded quality in sigma noughts and winds. The satellite attitude in ZGM is slightly degraded and the "old" ground processor was not able to produce calibrated data anymore. For that reason a re-design of the entire ground processing has been carried out and since August 21st 2003 the new processor named ERS Scatterometer Attitude Corrected Algorithm (ESACA) is operative in all the ESA ground station and data was redistributed to the user.
Although for a long period data was not distributed, the PCS has monitored the data quality (as shown in Figure 12) and the results during that period can be summarized as:

At the beginning of the ZGM (January 2001 - end July 2001) the number of valid nodes has clear drop from 190000 per day to 9000 per day. This because the satellite attitude was strong degraded and the received signal had a very high Kp figure (in particular for the far range nodes). For the valid nodes, due to no calibrated sigma nought, the quality of the wind was very poor, the distance from the cone was high and the wind speed bias was above 1.5 m/s.
At the end of July 2001 the ZGM has been tuned and the satellite attitude had an improvement. This explains the increase of the number of valid nodes (returned around the nominal level) and the improvements in the wind speed bias (around 0.5 m/s).
On 4th February 2003, a beta version of the new ESACA processor has been put in operation in Kiruna for validation and the monitoring of the data quality has been done only for the new ESACA data. The number of valid nodes slight decreased because Kiruna station process only 9 of 14 orbits per day. The wind speed direction deviation had a clear improvement because ESACA implements a new ambiguity removal algorithm (MSC) and the ambiguity removal rate is now stable at 100% (the MSC is able to remove ambiguity for all the nodes). The wind speed bias had a clear drop from 0.5 to -0.5 m/s. That value is closer to the nominal one (around -0.2 m/s). As reported in the previous cyclic reports the beta version of ESACA had some calibration problem for the near range nodes and this explains why the data quality does not match exactly the one obtained in the nominal YSM. That problem has been overcome with the final release of the ESACA processor put into operation on August 21st 2003. On June 22nd the failure of the on-board tape recorder discontinued the ERS global mission (see section 4.1) and this explains the low number of valid nodes available after that day.
The performances of ESACA winds delivered between August 2003 and September 2004 are affected by land contamination. Around costal zones many Sea nodes have a strong contribution of Land backscattering and the retrieved wind is not correct. An optimization of

the Land/Sea flag in the ground processing has been carried out during the cycle 98. In the statistics computed by PCS on the fast delivered winds the Land contamination has been removed by using a refined Land/Sea mask. Also the ice contamination has been removed with a simple geographical filter. With these new setting the PCS statistics are very similar to the ones reported by ECMWF.

For cycle 164 the wind performances was stable. The wind speed bias (UWI vs 18 or 24 hour forecast) was roughly 0.7 m/s and the speed bias standard deviation was around 1.7 m/s.

The wind direction deviation for cycle 164 was good with more than 98% of the nodes wind direction in agreement with the ECMWF forecast.

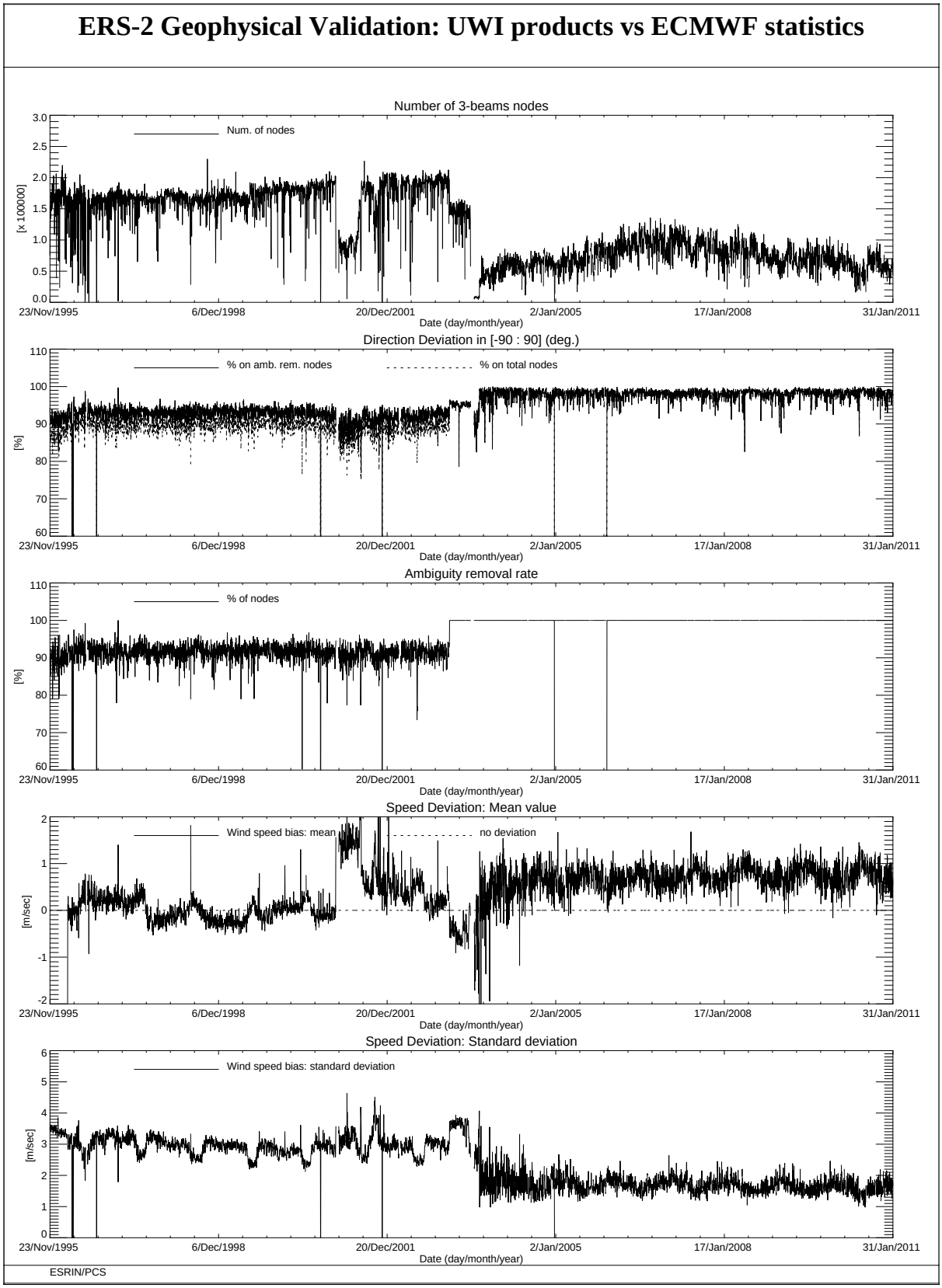

FIGURE 12 ERS-2 Scatterometer: wind products performance since the beginning of the mission.

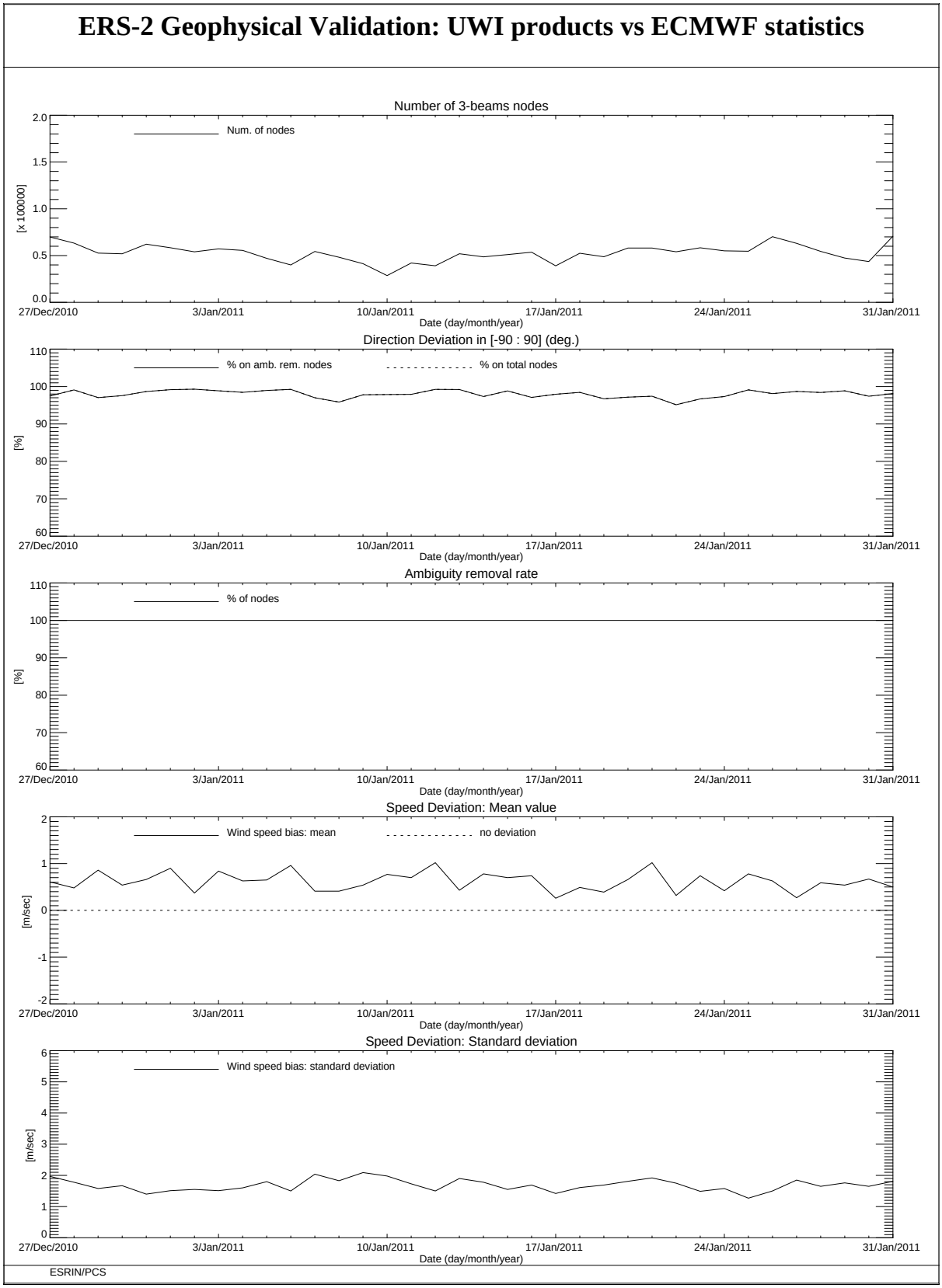

FIGURE 13 ERS-2 Scatterometer: wind products performance for cycle 164.

4.3 ECMWF Geophysical Monitoring

The quality of the UWI product was monitored at ECMWF for Cycle 164. Results were compared to those obtained from the previous Cycle, as well for data received during the nominal period in 2000 (up to Cycle 59). No corrections for duplicate observations from overlapping ground stations were applied.

During Cycle 164 data was received between 21:05 UTC 27 December 2010 and 20:59 UTC 31 January 2011. Data was grouped into 6-hourly batches (centred around 00, 06, 12 and 18 UTC). For all batches data was received.

Data is being recorded whenever within the visibility range of a ground station. For Cycle 164, data coverage was over the North-Atlantic, the Mediterranean, part of the Gulf of Mexico, an area in the Pacific west from the US, Canada and Central America and some data over the area in between Antarctica and Australia. In this latter region coverage was reduced with respect to Cycle 163.

Time series of the asymmetry between the fore and aft incidence angles shows a reasonably stable behaviour.

Compared to Cycle 163, the UWI wind speed relative to ECMWF first-guess (FG) fields showed a slightly higher standard deviation (1.52 m/s, was 1.48 m/s). Bias levels were a bit more negative (on average -0.86 m/s, was -0.84 m/s). Relative standard deviation for wind direction has improved (28.9 degrees, was 33.0 degrees).

Ocean calibration shows that inter-node and inter-beam dependencies of bias levels are similar. Average bias level was stable (-0.48 dB, was -0.54 dB).

The ECMWF operational assimilation and forecast system was not changed during Cycle 164. The Cycle-averaged evolution of performance relative to ECMWF first-guess (FG) winds is displayed in Figure 14. Figure 15 shows global maps of the over Cycle 164 averaged UWI data coverage and wind climate, Figure 16 for performance relative to FG winds.

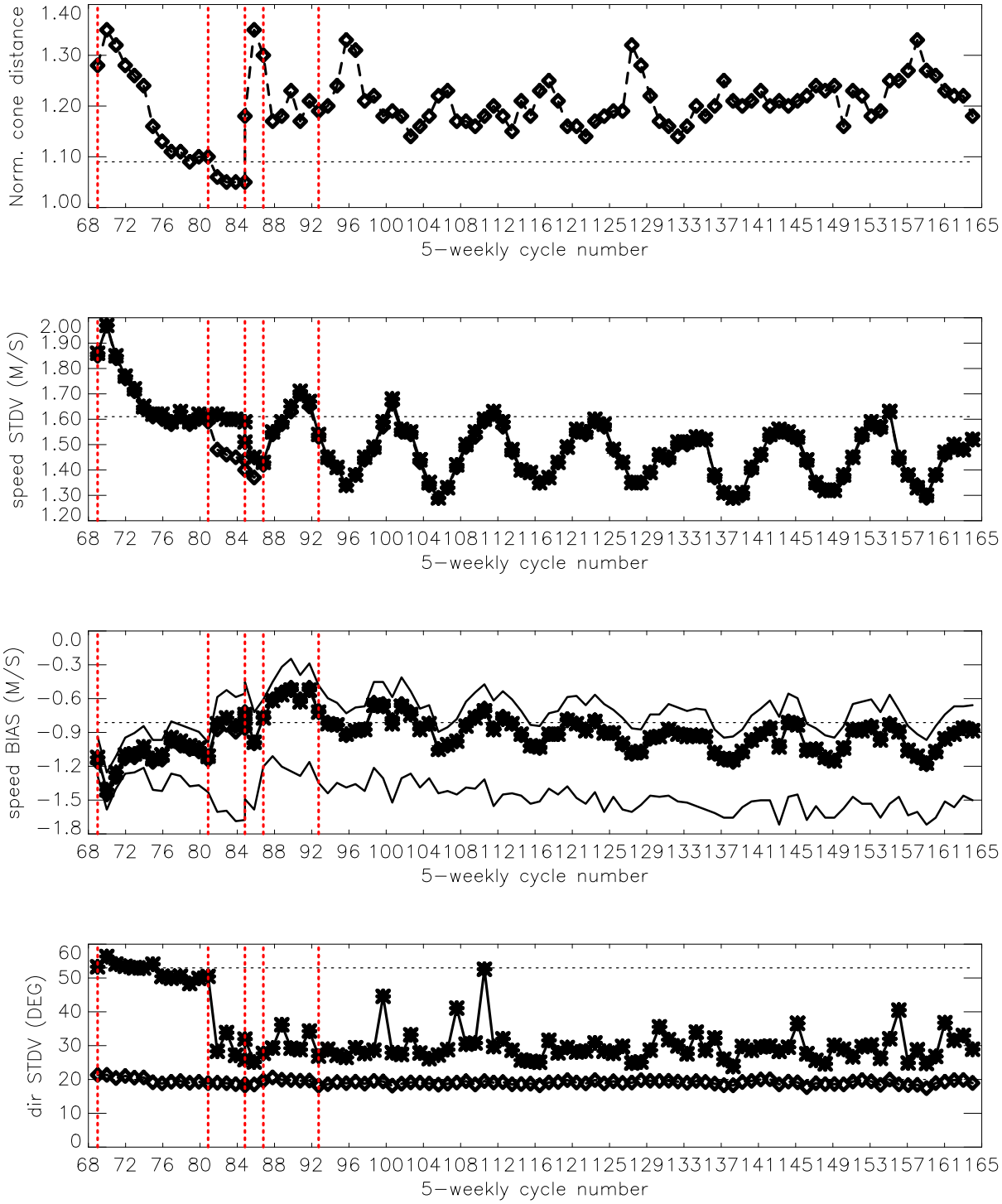

FIGURE 14 Evolution of the performance of the ERS-2 scatterometer averaged over 5-weekly Cycles from 12 December 2001 (Cycle 69) to 31 January 2011 (end Cycle 164) for the UWI product (solid, star) and de-aliased winds based on CMOD4 (dashed, diamond). Results are based on data that passed the UWI QC flags. For Cycle 85 two values are plotted; the first value for a global set, the second one for a regional set (for details see the corresponding cyclic report). Dotted lines represent values for Cycle 59 (5 December 2000 to 17 January 2001), i.e. the last stable Cycle of the nominal period. From top to bottom panel are shown the normalized distance to the cone (CMOD4 only) the standard deviation of the wind speed compared to FG winds, the corresponding bias (for UWI winds the extremes in node-wise averages are shown as well), and the standard deviation of wind direction compared to FG.

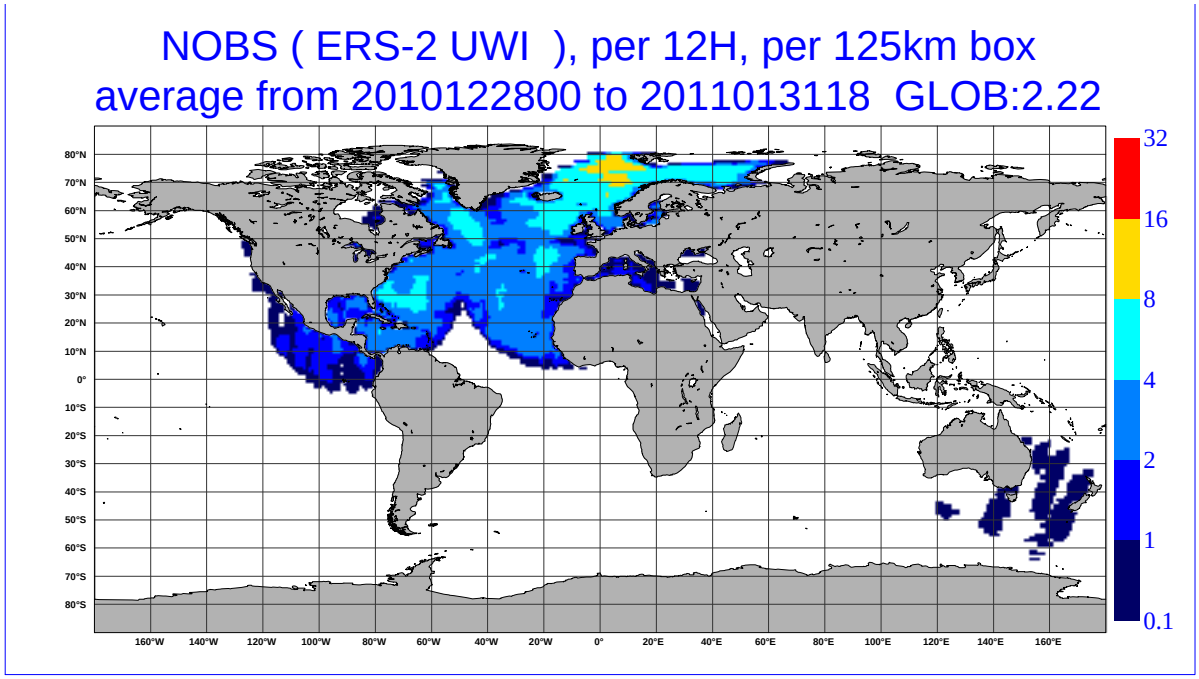

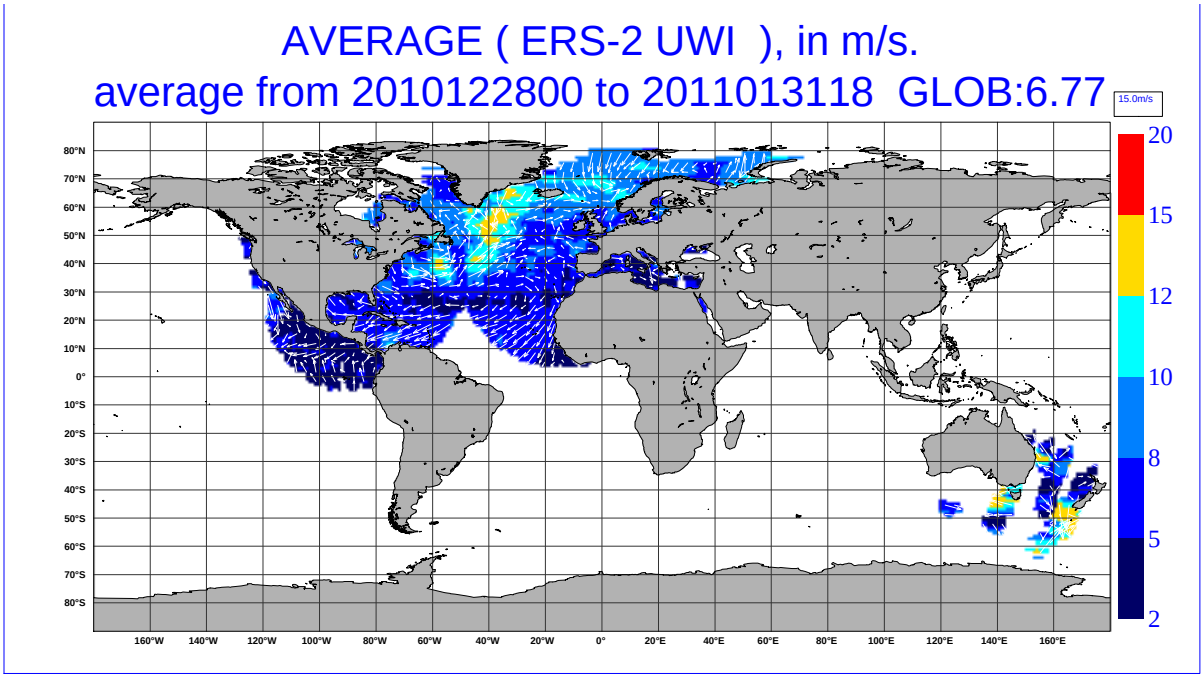

FIGURE 15 Average number of observations per 12H and per 125km grid box (top panel) and wind-climate (lower panel) for UWI winds that passed the UWI flags QC and a check on the collocated ECMWF land and sea-ice mask.

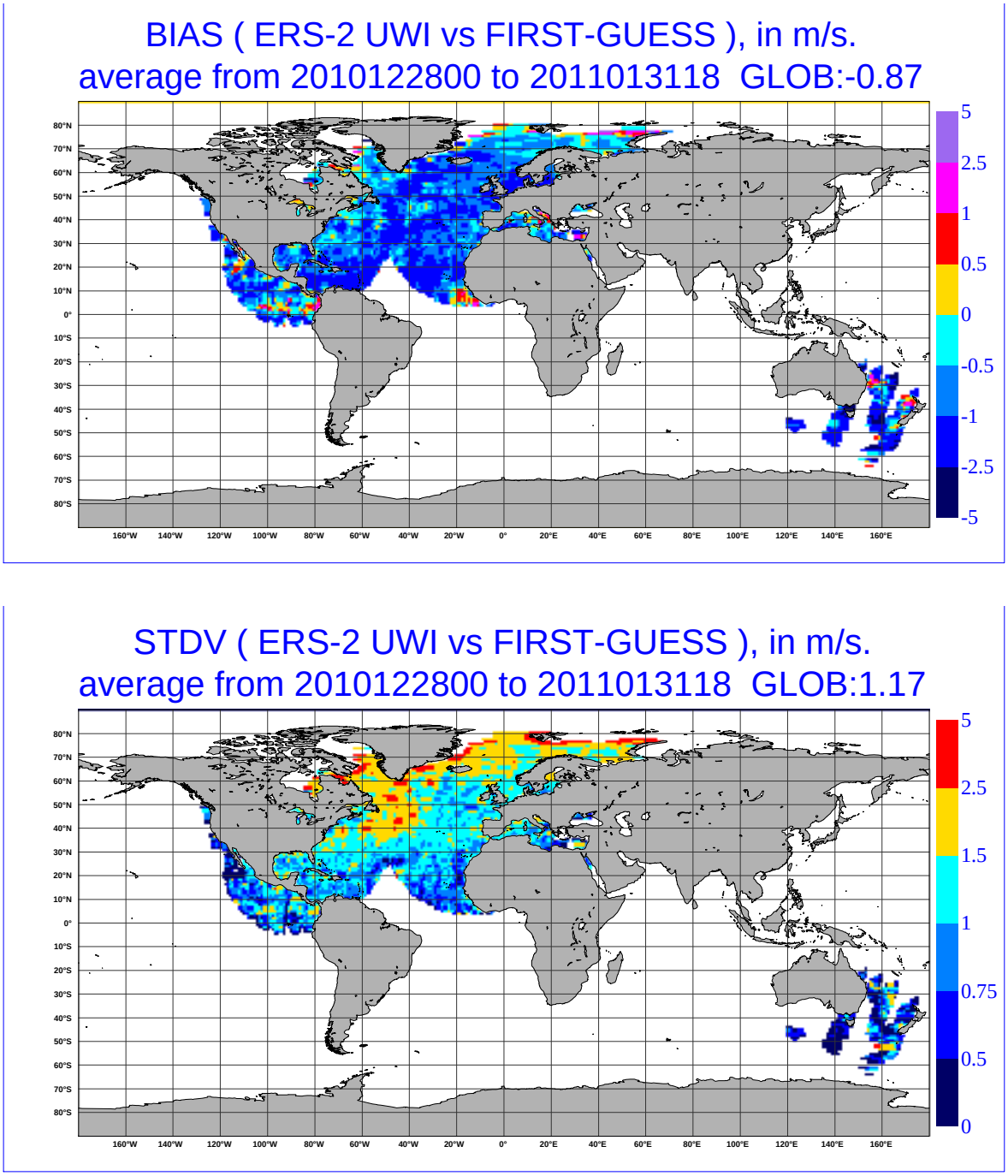

FIGURE 16 The same as Figure 15, but now for the relative bias (top panel) and standard deviation (lower panel) with ECMWF first-guess winds.

4.3.1 Distance to cone history

The distance to the cone history is shown in Figure 17. Curves are based on data that passed all QC, including the test on the k_p-yaw flag, and subject to the land and sea-ice check at ECMWF (see cyclic report 88 for details).

Like for previous Cycles, time series are (due to lack of statistics) very noisy, especially for the near-range nodes. Most spikes were found to be the result of low data volumes.

Compared to Cycle 163, the average level was lower (1.18, was 1.22), and is higher (by 8%) than for nominal data (see top panel Figure 14).

The fraction of data that did not pass QC is displayed in Figure 17 as well (dashed curves).

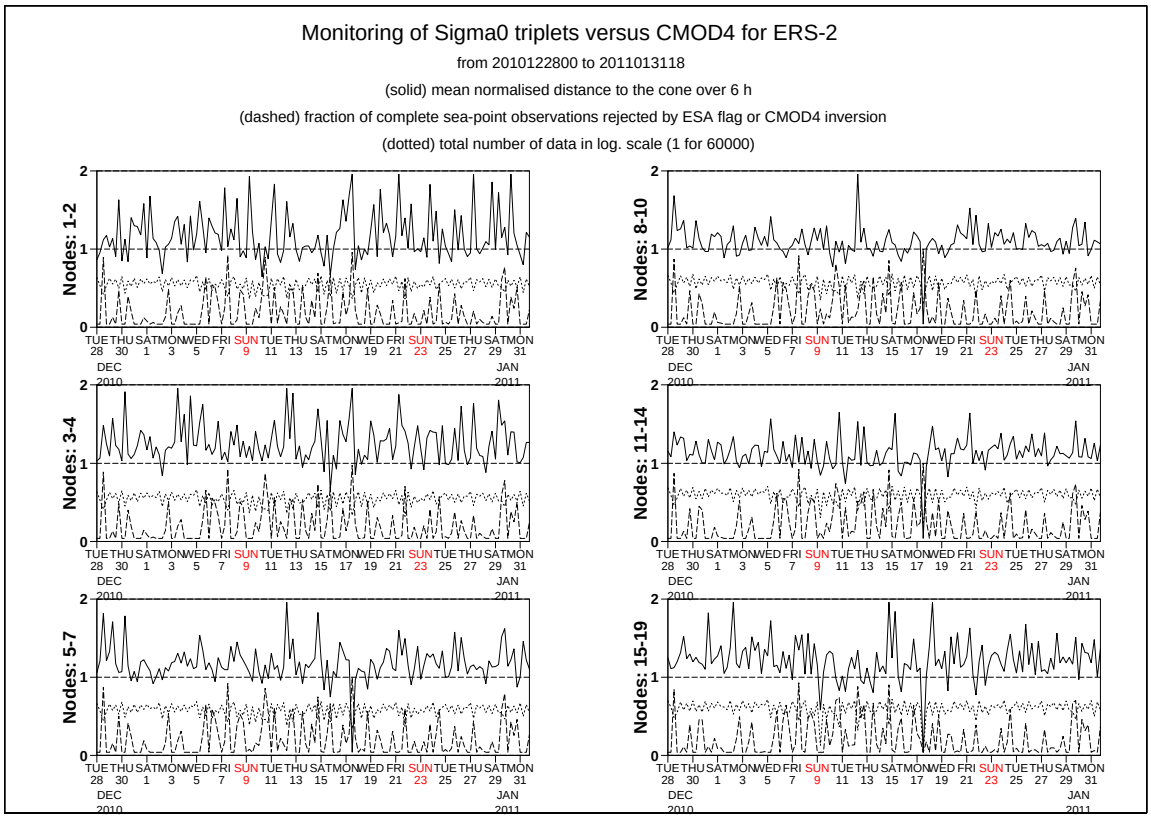

FIGURE 17 Mean normalized distance to the cone computed every 6 hours for nodes 1-2, 3-4, 5-7, 8-10, 11-14 and 15-19). The dotted curve shows the number of incoming triplets in logarithmic scale (1 corresponds to 60,000 triplets) and the dashed one indicates the fraction of complete (based on the land and sea-ice mask at ECMWF) sea-located triplets rejected by ESA flags, or by the wind inversion algorithm (0: all data kept, 1: no data kept).

4.3.2 UWI minus First-Guess history

In Figure 18, the UWI minus ECMWF first-guess wind-speed history is plotted. The history plot shows a few peaks, which are usually the result of low data volume.

Figure 22 displays the locations for which UWI winds were more than 8 m/s weaker (top panel), respectively more than 8 m/s stronger (lower panel) than FG winds. Like for Cycle 163, such collocations are isolated, and often indicate meteorologicaly active regions, for which UWI data and ECMWF model field show reasonably small differences in phase and/or intensity. Deviations near the poles are the result of imperfect sea-ice flagging.

Two examples for which UWI and ECMWF winds differ significantly are presented in Figure 23. Both panels show the case of a slight shift in a front over the Atlantic.

Average bias levels and standard deviations of UWI winds relative to FG winds are displayed in Table 6. From this it follows that the bias of UWI winds was slightly less negative (-0.84 m/s, was -0.89 m/s), being around the level of nominal data in 2000.

Table 6 Wind speed and direction biases

	Cycle 163		**Cycle 164**	
	UWI	CMOD4	UWI	CMOD4
Speed STDV	1.48	1.48	1.52	1.52
Node 1-2	1.57	1.53	1.58	1.56
Node 3-4	1.48	1.47	1.5	1.49
Node 5-7	1.43	1.43	1.44	1.44
Node 8-10	1.42	1.42	1.45	1.45
Node 11-14	1.43	1.43	1.48	1.49
Node 15-19	1.45	1.46	1.52	1.53
Speed BIAS	-0.84	-0.83	-0.86	-0.85
Node 1-2	-1.42	-1.39	-1.46	-1.42
Node 3-4	-1.13	-1.08	-1.17	-1.12
Node 5-7	-0.86	-0.83	-0.9	-0.86
Node 8-10	-0.68	-0.67	-0.7	-0.7
Node 11-14	-0.65	-0.65	-0.64	-0.65
Node 15-19	-0.66	-0.68	-0.64	-0.66

Direction STDV	33.00	19.80	28.90	18.90
Direction BIAS	-2.00	-2.10	-2.90	-2.90

On a longer time scale seasonal bias trends are observed (see Figure 14). As was highlighted in previous cyclic reports, it is believed that the yearly trend is partly induced by changing local geophysical conditions.

The standard deviation of UWI wind speed versus ECMWF FG was, compared to Cycle 162, slightly higher (1.52 m/s, was 1.48 m/s).

For Cycle 164 the (UWI - FG) direction standard deviations were mostly ranging between 20 and 40 degrees (Figure 20). Average STDV for UWI wind direction significantly lower than for Cycle 163 (28.9 degrees, was 33.0 degrees). For at ECMWF de-aliased winds (Figure 21) performance is better as well (STDV 18.9, was 19.8 degrees).

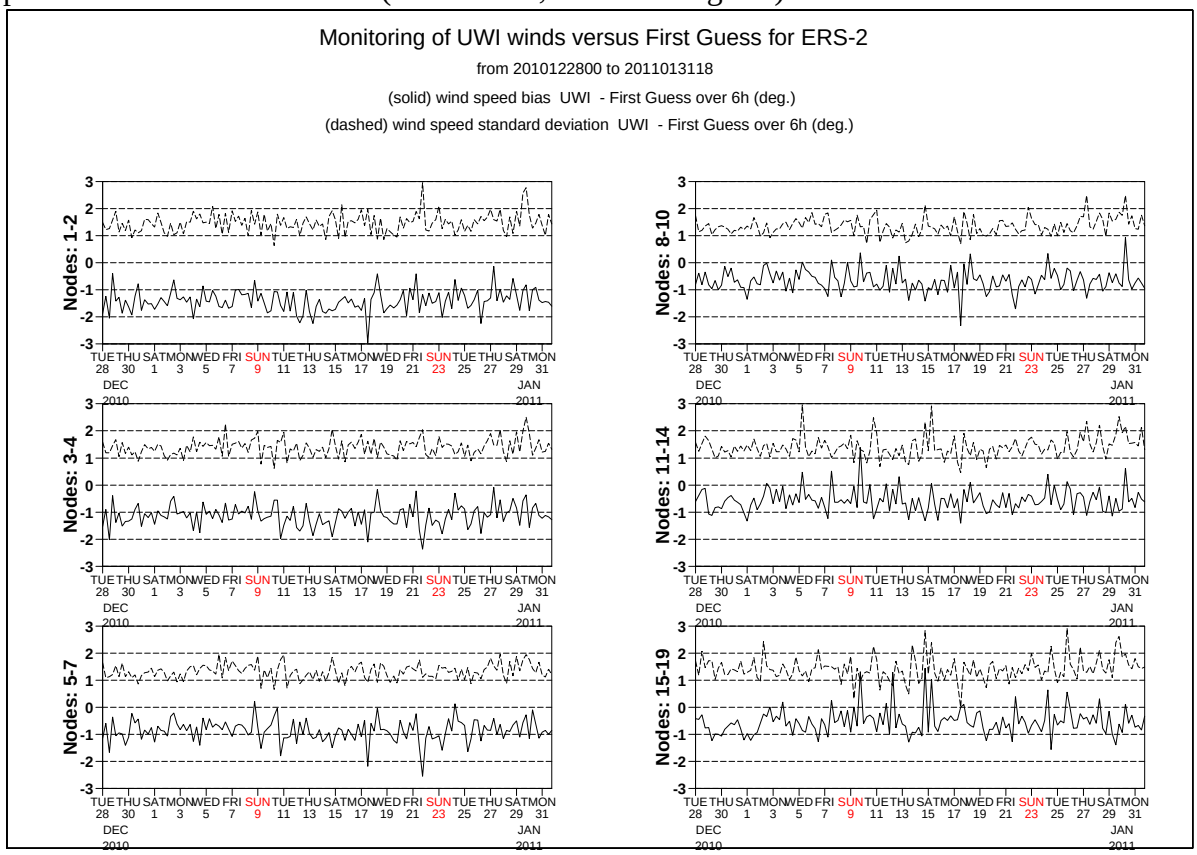

FIGURE 18 Mean (solid line) and standard deviation (dashed line) of the wind speed difference UWI - first guess for the data retained by the quality control.

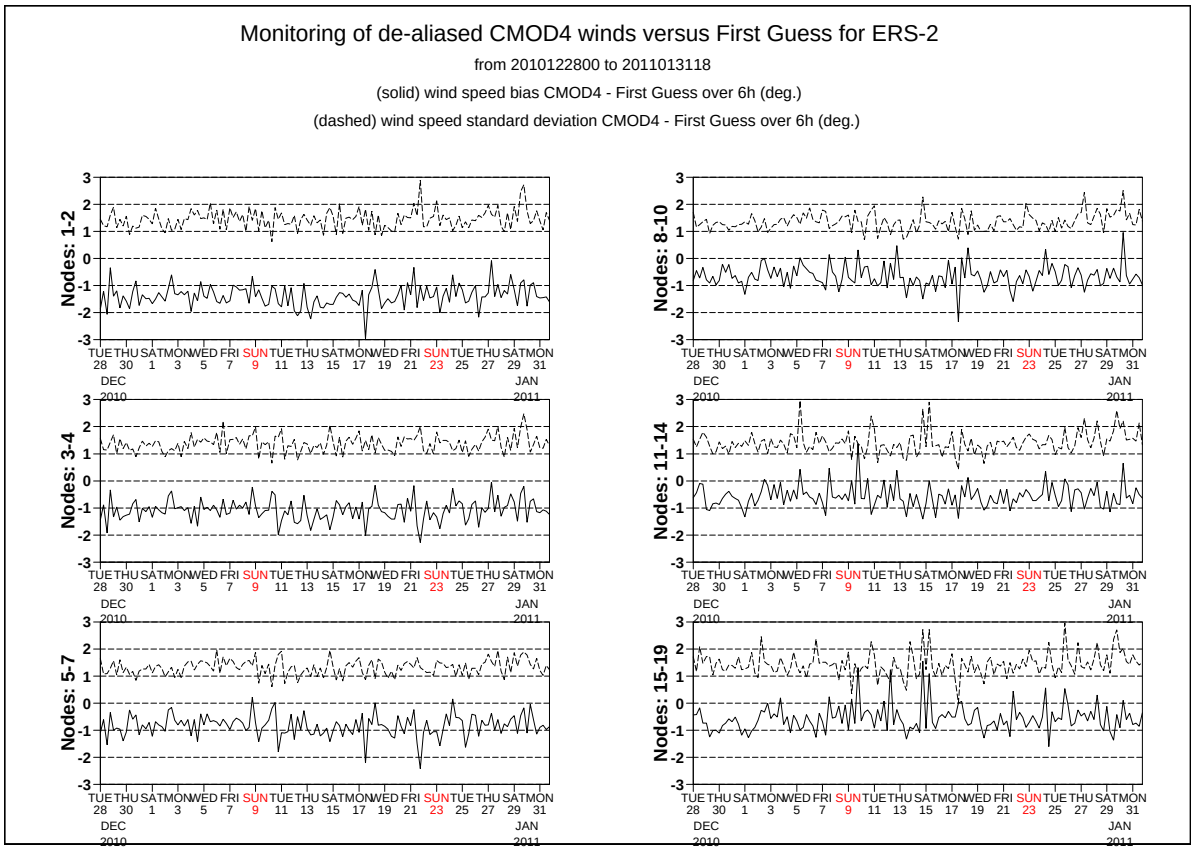

FIGURE 19 Same as Fig. 18, but for the de-aliased CMOD4 data.

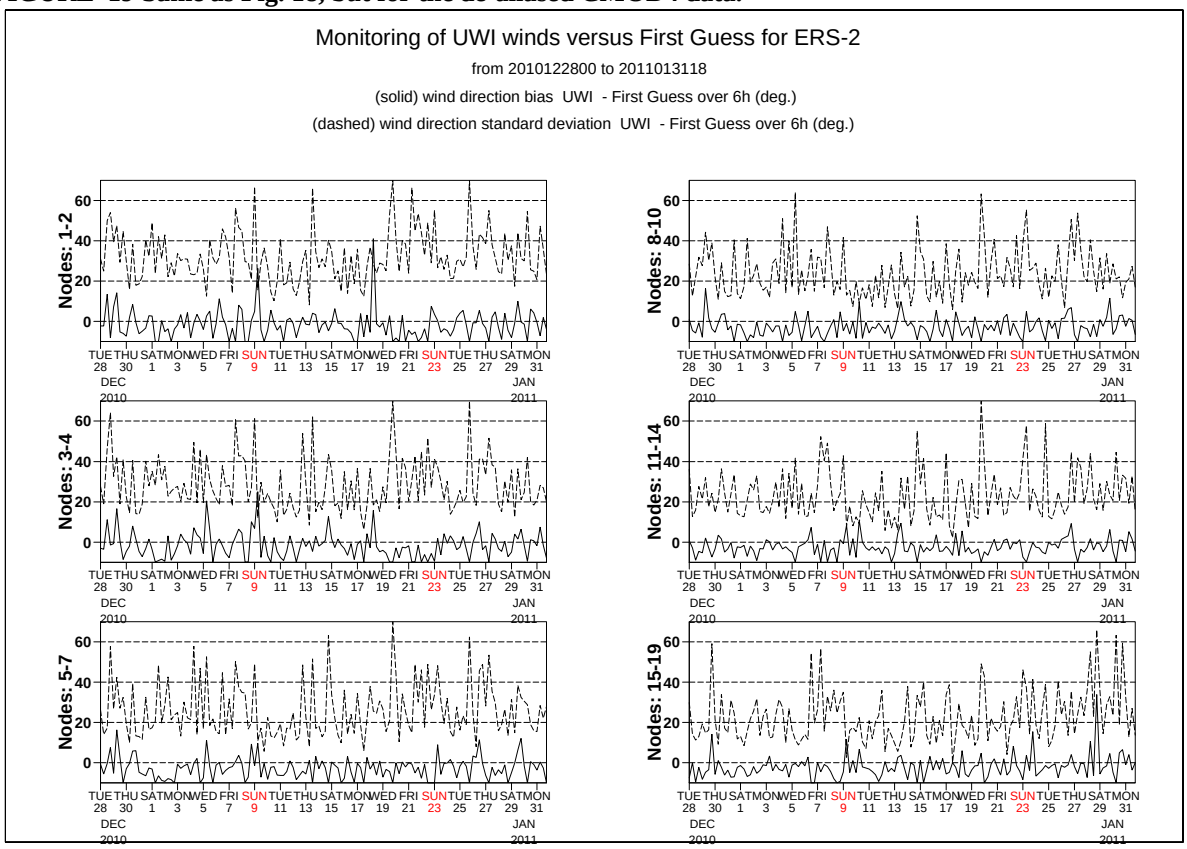

FIGURE 20 Same as Fig. 18, but for the wind direction difference. Statistics are computed only for wind speeds higher than 4 m/s.

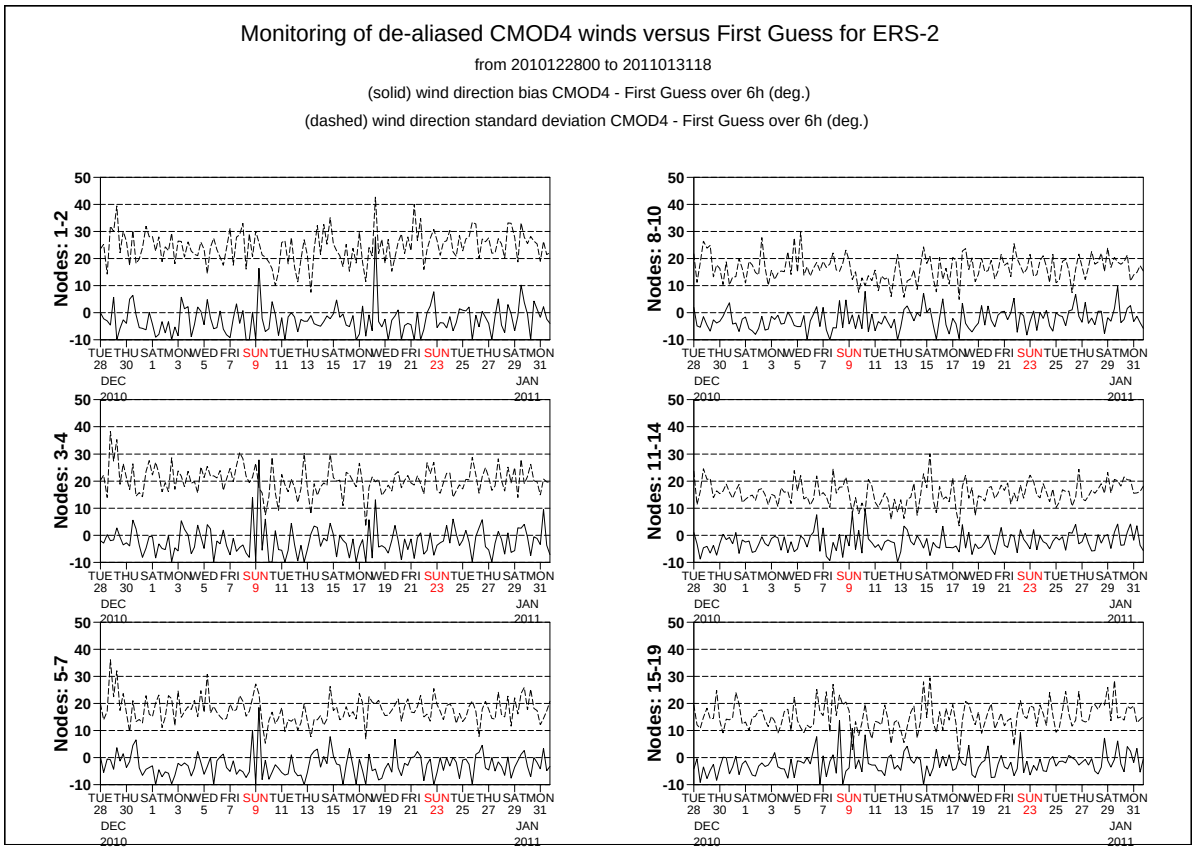

FIGURE 21 Same as Fig. 20, but for the de-aliased CMOD4 data.

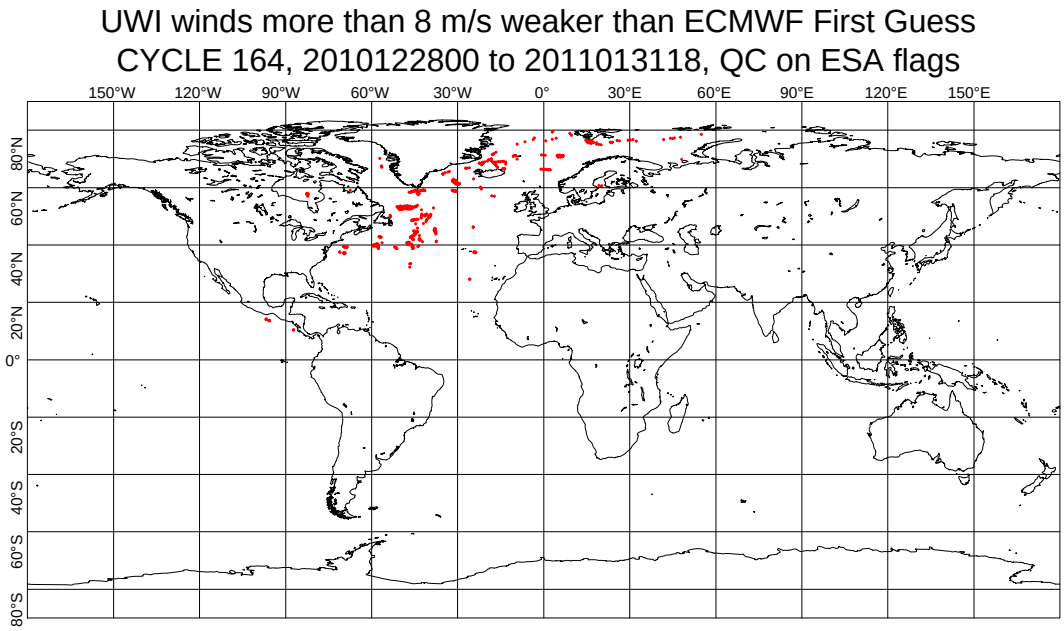

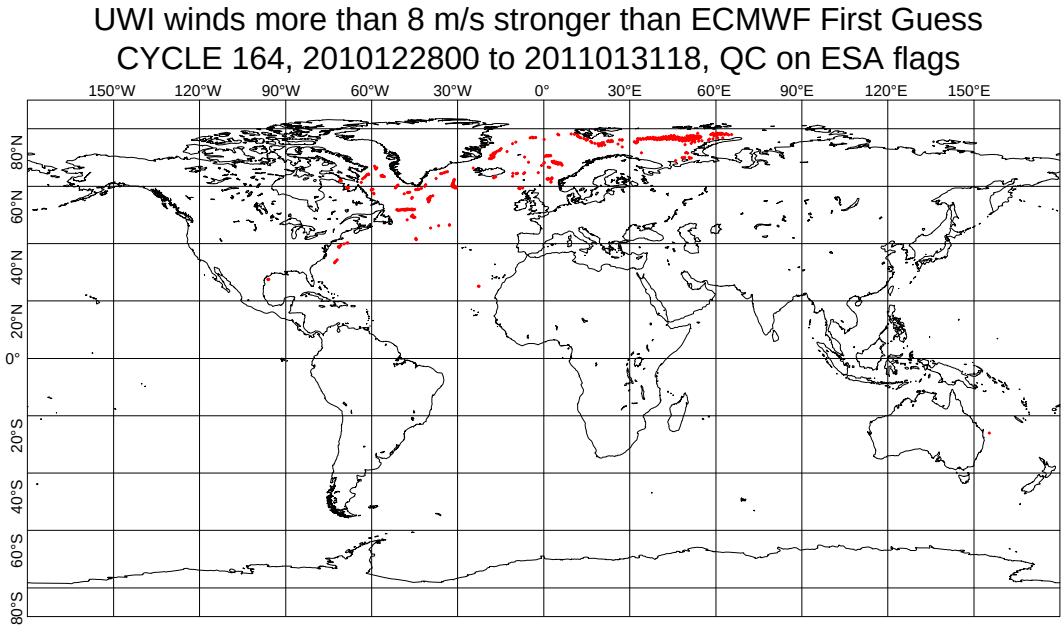

FIGURE 22 Locations of data during cycle 164 for which UWI winds are more than 8 m/s weaker (top panel) respectively stronger (lower panel) than FGAT, and on which QC on UWI flags and the ECMWF land/sea-ice mask was applied.

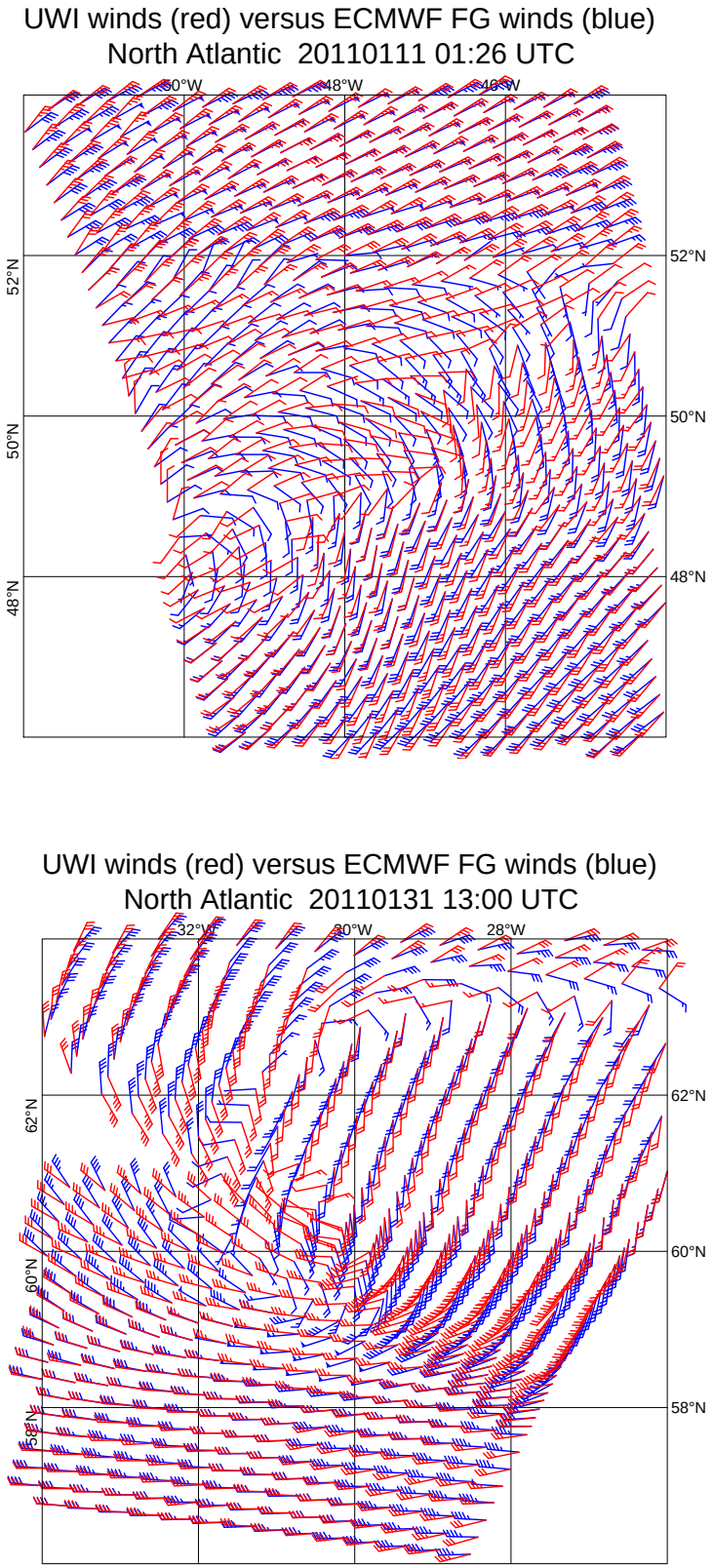

FIGURE 23 A case in the North Atlantic on 11 January (top panel) and a case in North Atlantic for 31 January 2011 (lower panel). Red and blue barbs represent UWI winds and ECMWF FG winds, espectively.

4.3.3 Scatter plots

Scatterplots of FG winds versus ERS-2 winds are displayed in Figures 24 to 27. Values of standard deviations and biases are slightly different from those displayed in Table 6. Reason for this is that, for plotting purposes, the in 0.5 m/s resolution ERS-2 winds have been slightly perturbed (increases scatter with 0.02 m/s), and that zero wind-speed ERS-2 winds have been excluded (decreases scatter with about 0.05 m/s).

The scatter plot of UWI wind speed versus FG (Figure 24) is very similar to that for (at ECMWF inverted) de-aliased CMOD4 winds (Figure 26). It confirms that the ESACA inversion scheme is working properly.

Winds derived on the basis of CMOD5 are displayed in Figure 27. The relative standard deviation is lower than for CMOD4 winds (1.49 m/s versus 1.54 m/s). Compared to ECMWF FG, CMOD5 winds are 0.33 m/s slower.

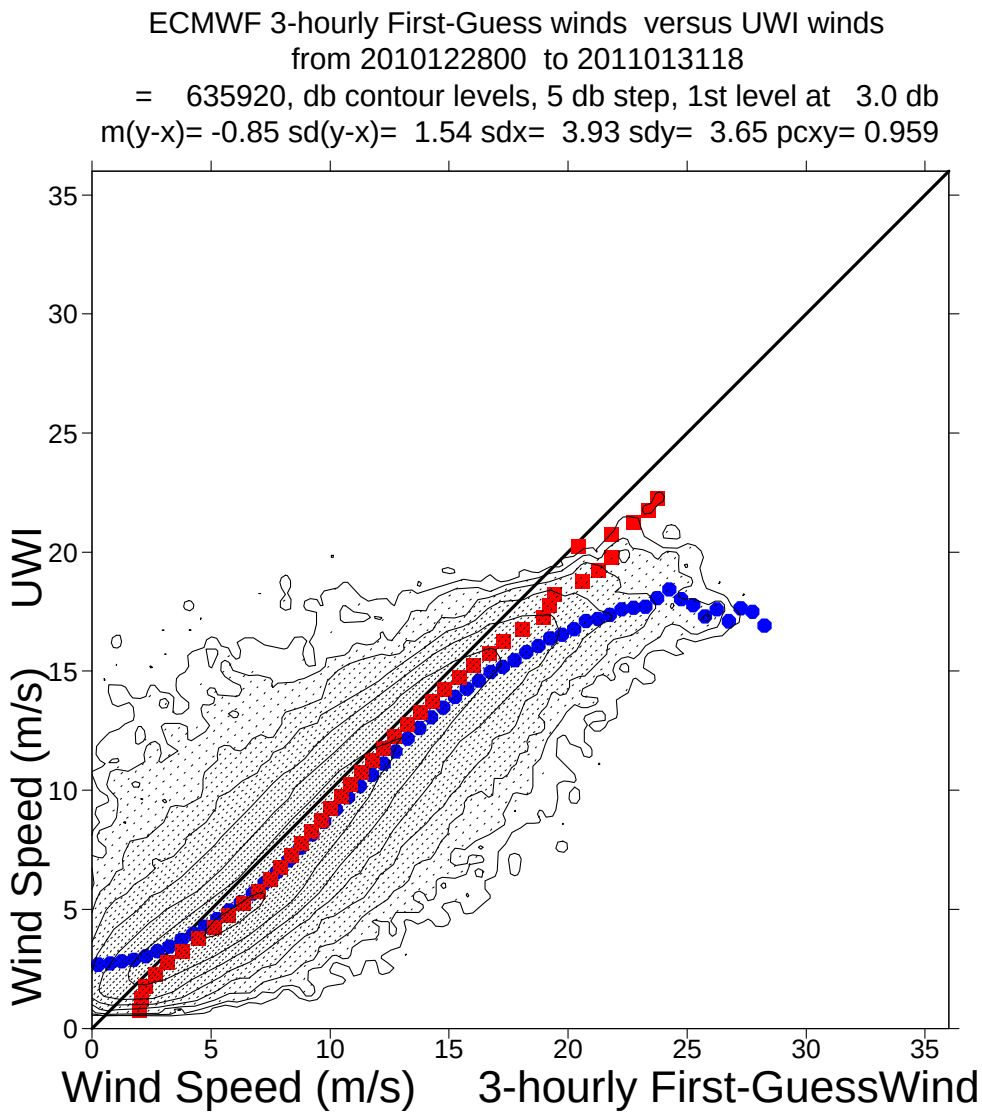

FIGURE 24 Two-dimensional histogram of first guess and UWI wind speeds, for the data kept by the UWI flags, and QC based on the ECMWF ice and land and sea-ice mask. Circles denote the mean values in the y-direction and squares those in the x-direction.

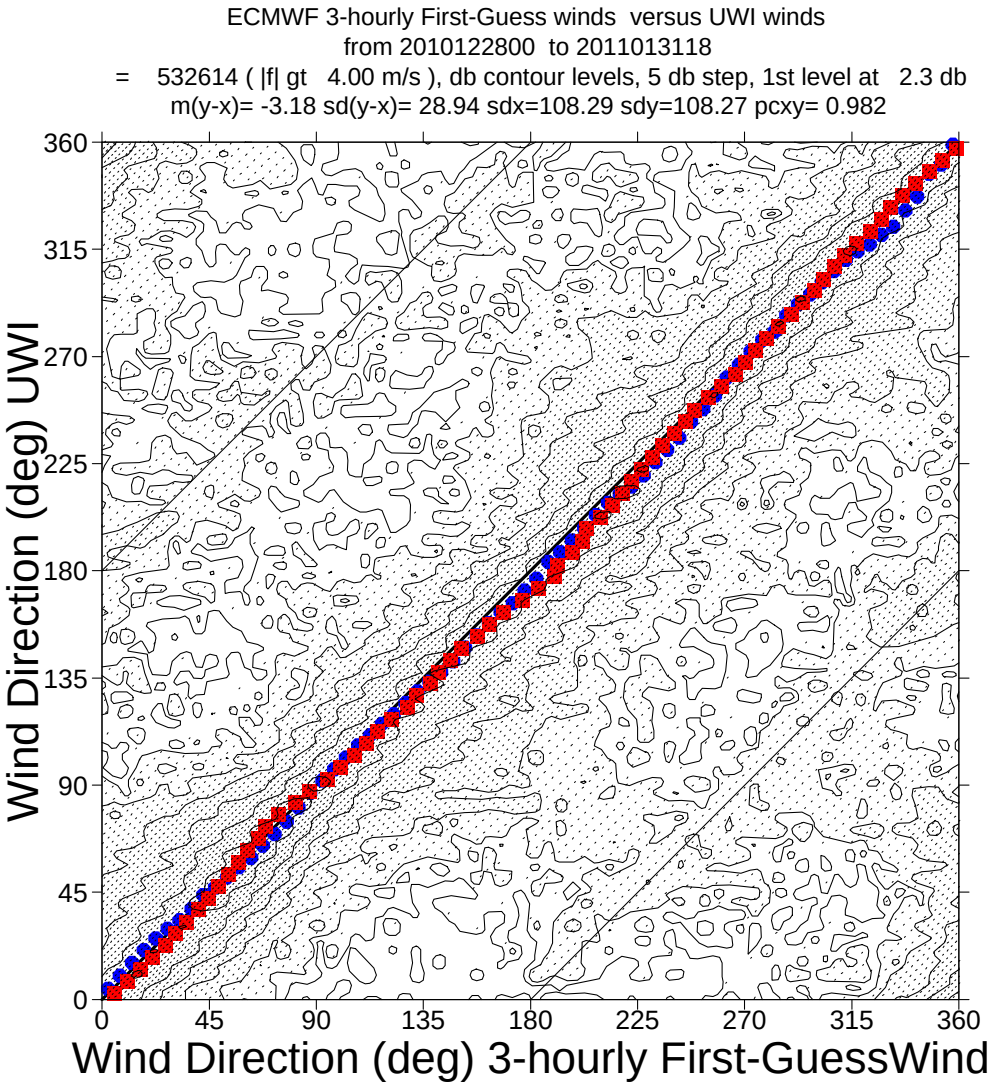

FIGURE 25 Same as Fig. 24, but for wind direction. Only wind speeds higher than 4m/s are taken into account.

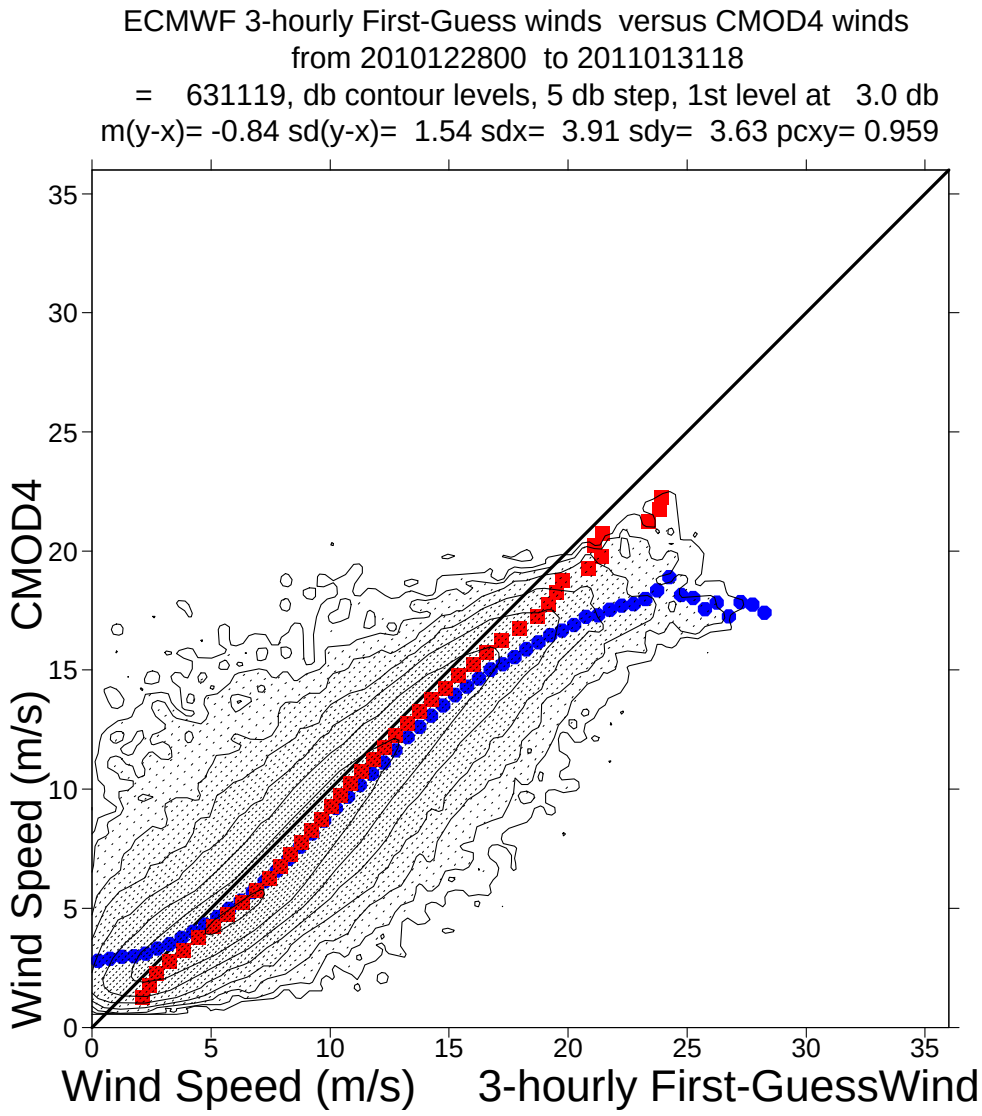

FIGURE 26 Same as Fig. 24, but for de-aliased CMOD4 winds.

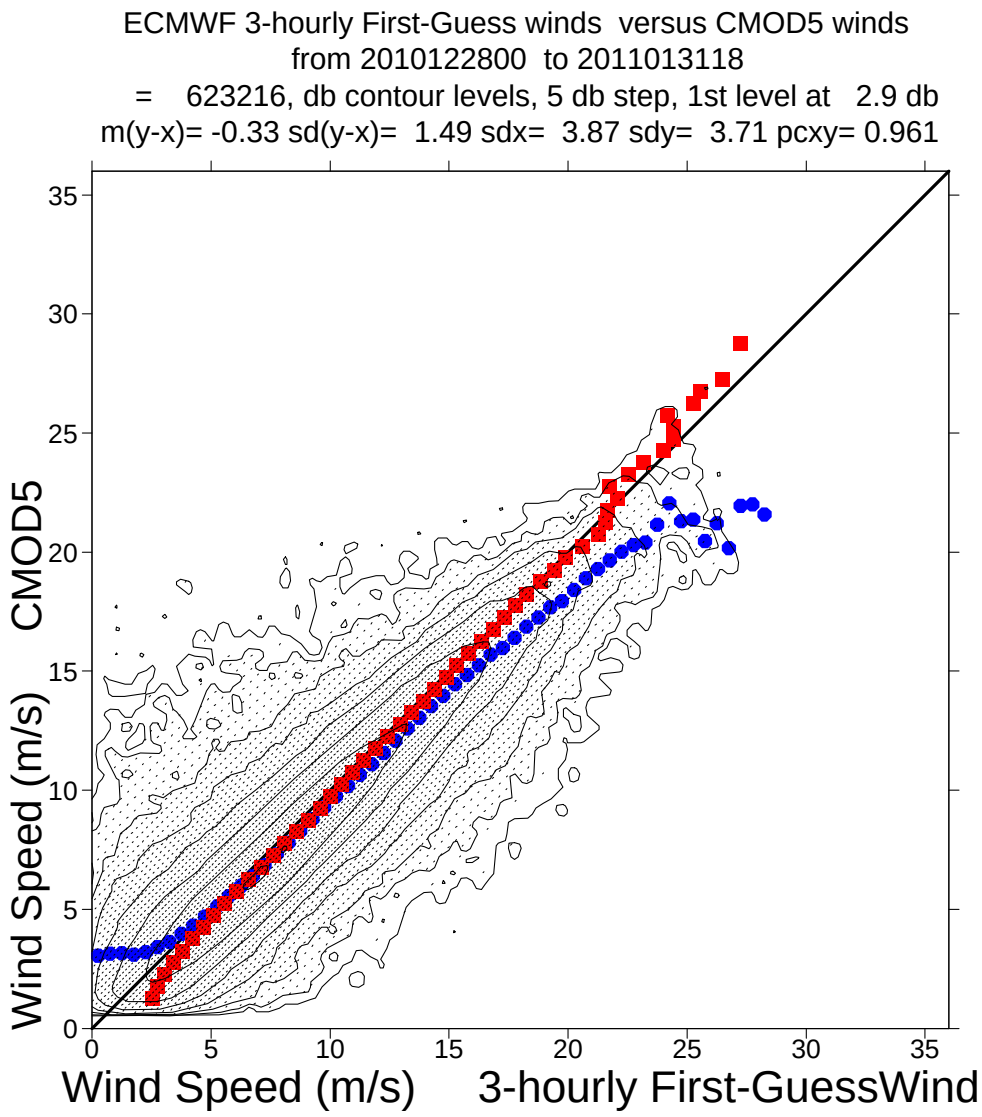

FIGURE 27 Same as Fig. 24, but for de-aliased CMOD5 winds.

4.4 Timeliness evolution

The Scatterometer product timeliness is defined as the difference between the acquisition time of the first product and the creation date of the file received in ESRIN-PCS. Once the UWI file is received in ESRIN, data are converted in BUFR format and sent to users via the GTS network. Therefore that timeliness is an indicator of the delay time that the user could expect in the data dissemination. The analysis does not take into account delays in the GTS network. For each file received from the ground station, the timeliness is computed and this analysis reports the daily mean timeliness obtained by averaging all the values.
The analysis has been performed on the daily timeliness average. Timeliness is zero when no products are received.

In the next figures is showed the evolution of the daily mean timeliness of Kiruna, Maspalomas, Gatineau, West Freugh and Miami stations since April 2005. Since 2007 the analysis has been extended also first to McMurdo and Beijing products and then to Matera, Hobart, Singapore and Chetumal products. The starting date of the analysis, for each station, is reported in the following table:

TABLE 6 Starting date of Timeliness analysis for each station

STATION	START DATE
Kiruna	19 April 2005
Gatineau	19 April 2005
Maspalomas	19 April 2005
West Freugh	19 April 2005
Miami	19 April 2005
McMurdo	13 March 2007
Beijing	13 March 2007
Matera	5 December 2007
Hobart	5 December 2007
Singapore	5 December 2007
Chetumal	5 December 2007
Johannesburg	17 July 2008

The Figure 28 shows the results of the investigation for Gatineau, Kiruna, Maspalomas, Matera and Singapore stations.

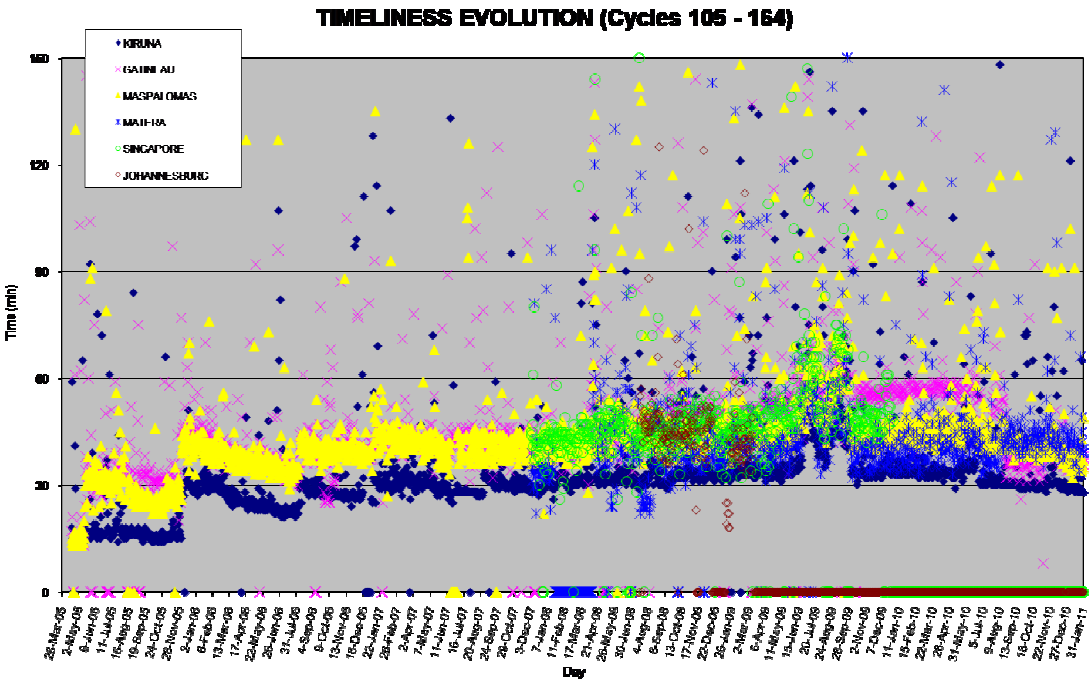

FIGURE 28 Timeliness evolution from 19th April 2005 to 31st January 2011 for Kiruna, Gatineau, Maspalomas, Matera, Singapore, and Johannesburg ground stations.

Apart from some values out of the general tendency due to temporary system or connection problem, since the beginning of the analyzed period a timeliness increase is detected for Kiruna, Maspalomas and Gatineau stations. In particular, it can be recognized a discontinuous trend for the three stations with quickly increases in the same days for the 3 stations followed by a slightly decrease in the subsequent months. In depth analysis showed that these rapid increases occur about in the following days: 5 May 2005, 5 December 2005, 9 August 2006 and 9 January 2007. This behavior could be due to settings modifications in the ground segment. A general degradation of the timeliness performances occurred from the end of June 2009 to September 2009.

During cycle 164 the timeliness performances stayed stable for most of the stations, apart from the periods affected by unavailability (January 4th). In the reporting period Kiruna showed a stable mean timeliness of 30 minutes. Maspalomas, Gatineau, and Matera had a mean value of about 40 minutes. No relevant information on Johannesburg and Singapore stations due to missing data for the reporting period.

The analysis for West Freugh, Miami, Beijing, McMurdo, Hobart and Chetumal stations is showed in Figure 29.

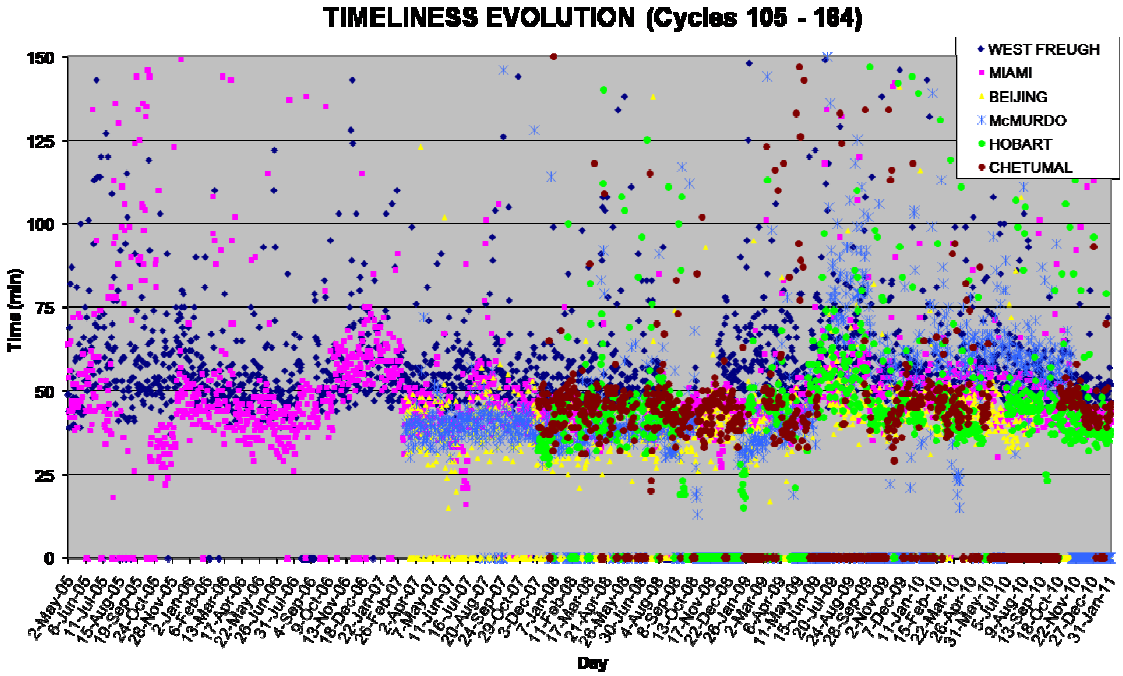

FIGURE 29 : Timeliness evolution from 19th April 2005 to 31st January 2011 for West Freugh, Miami, Beijing, McMurdo, Hobart, and Chetumal ground stations.

West Freugh and Miami stations show a similar regular trend in the analyzed period. More in detail a slightly increased timeliness could be identified since October 2006 followed by a decrease since January 2007. A general degradation of the timeliness performances occurred from the end of June 2009 to September 2009.

During the reporting period the timeliness performances stayed stable, apart from the periods affected by unavailability (January 4th). Miami and Chetumal had a mean value of about 40 minutes. West Freugh timeliness was about 50 minutes. No relevant information on McMurdo Hobart, and Beijing stations due to missing data for the reporting period.

The analysis carried out shows that till December 5th 2005 UWI products delivered from the three ESA ground station (Kiruna, Maspalomas, Gatineau) had a timeliness that fulfils the requirements for nowcasting application (data received on average within 25 minutes). After that date performances progressively degraded. During the reporting period the mean values for these stations was 30 minutes (Kiruna) and 40 minutes (Maspalomas and Gatineau). Therefore no more stations cover the requirements for nowcasting applications.

5 Yaw error angle estimation

The yaw error angle estimation is computed on-ground by the ESACA processors. The full set of results of the yaw processing is stored in an internal ESA product named HEY (Helpful ESA Yaw) disseminated from the ground station to ESRIN. The estimation of the yaw error angle is based on the Doppler shift measured on the received echo. That estimation can be done with a good accuracy only for small yaw error angle (in the range between +/-4 deg.). Above that range, due to high Doppler frequency shift the signal spectrum is outside the receiver bandwidth and the yaw estimation is strong degraded. Details regarding the yaw processing can be found on the following document (chapter 9): http://earth.esa.int/pcs/ers/scatt/articles/soamain-030521.pdf .

The yaw error angle estimation aims to compute the correct acquisition geometry for the three Scatterometer antenna throughout the entire orbit. The Yaw error angle information is used in the radar equation to derive the calibrated backscattering (sigma nought) from the Earth surface and to select the echo samples associated to one node. In ESACA the definition of the node position is as the one adopted in the old processor (for details see:.http://earth.esa.int/pcs/ers/scatt/articles/scatt_work98_processing.pdf). In such way the distance between the nodes (both along and across track) is kept constant (25 Km) and what is changing in function of the yaw error angle is the number of echo samples that contributes to the node calculation and the incidence angle of the measurement. This because the three Scatterometer antennae could see the node with a different geometry due to an arbitrary variation of the yaw angle along track. The number of samples that actually contributes to a node and the yaw flag can be retrieved from the UWI Data Set Record (DSR) product. For that reason the definition of few fields in the UWI product has been updated. For details see the Scatterometer cyclic report - cycle 90 -. The Figure 31 (since beginning of HEY dissemination) and Figure 32 (cycle) show for each orbit the average Doppler frequency shift (first 3 plots Fore Mid and Aft antenna), the minimum, maximum and mean yaw (fourth plot), the yaw standard deviation (fifth plot) and the percentage of source packets acquired with a yaw error angle outside the range +/- 2 degrees (sixth plot). On average the yaw evolution is within the specification for the ESACA processor to assure calibrated data. The evolving yaw bias occurred in June 2004 has been reported to the flight segment and corrective actions have been put in place to compensate for.

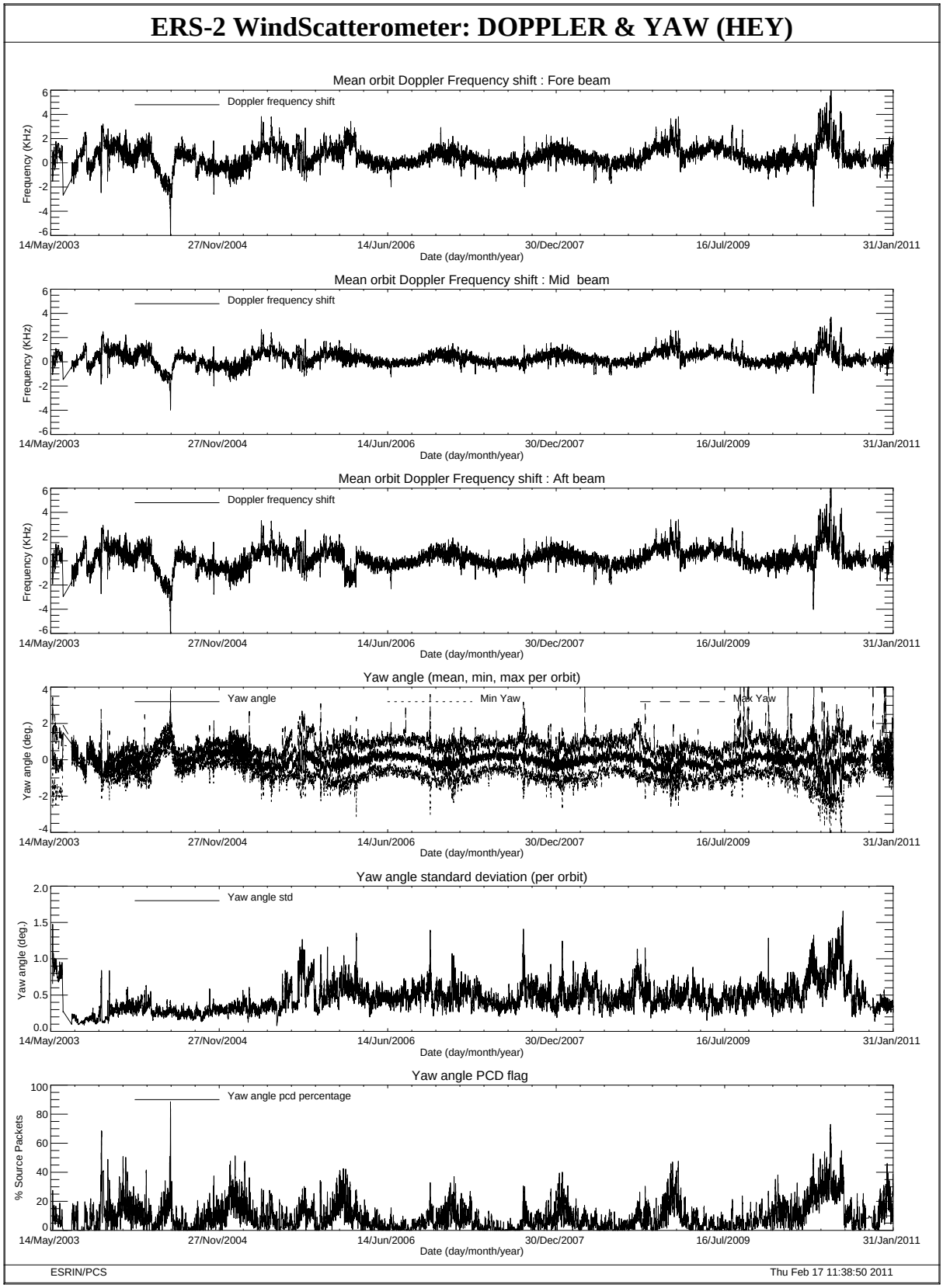

FIGURE 30 Doppler frequency shift and Yaw error angle evolution since August 2003 with a smooth of 14 orbits

The result of the monitoring for cycle 164 is an average (per orbit) yaw error angle within the expected nominal range (+/- 2 degrees) for most of the orbits. From Mid November a limited amount of Yaw angle data was available due to limited acquisitions in some ground stations.

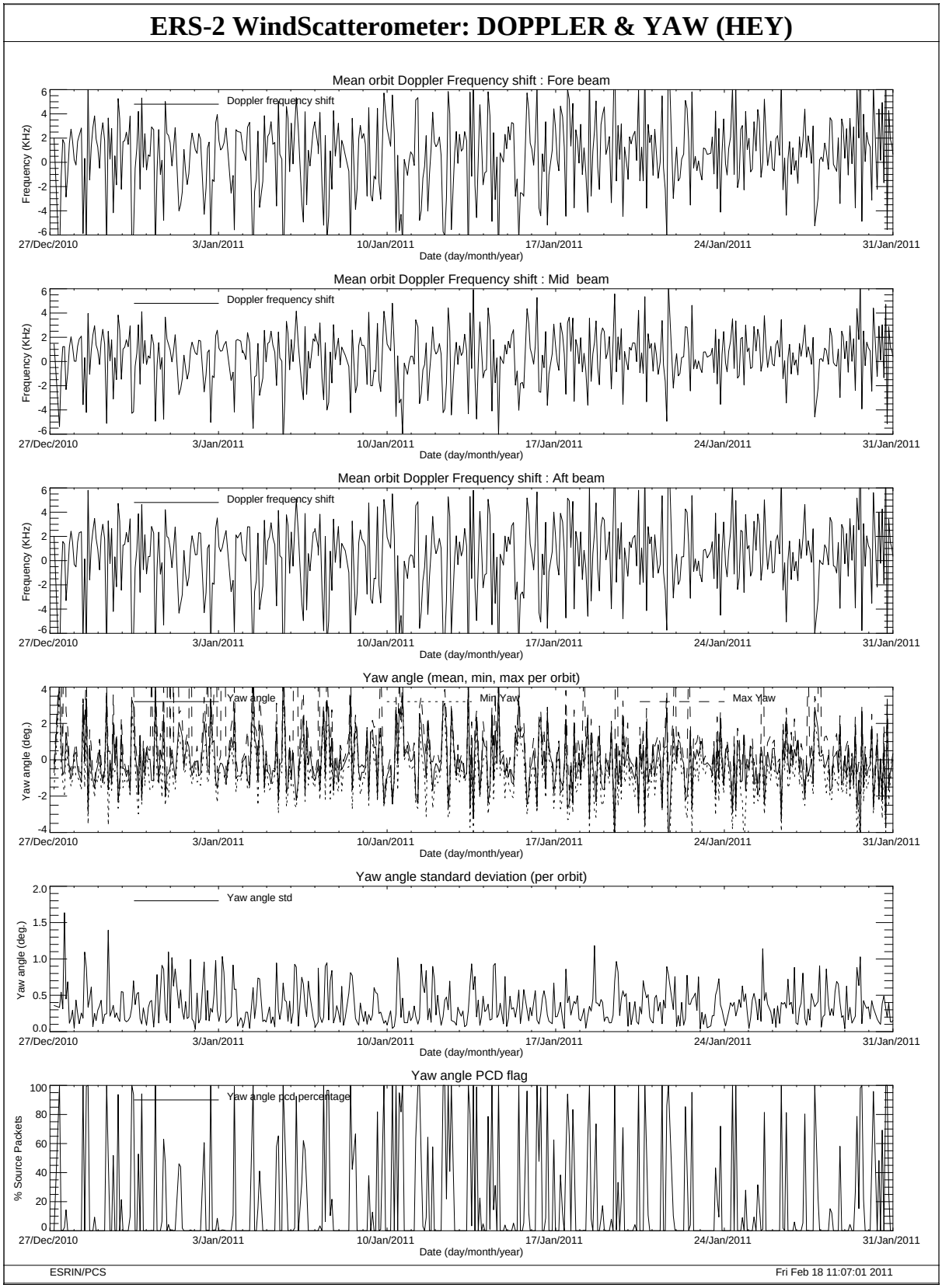

FIGURE 31 Doppler frequency shift and Yaw error angle evolution cycle 164.

5.1 Degraded Scatterometer Measurements

In case the YAW error angle is not computed due to a degraded attitude or it is out of the nominal range, the scatterometer measurements (sigma nought) are considered degraded and, for some applications, rejected.

The analysis of the degraded sigma nought measurements has been computed since cycle 149.

The statistics is performed on a daily base. The percentage of nodes with YAW not computed or out of limits among all nodes with at least one sigma nought measurements is computed (Fig. 32).

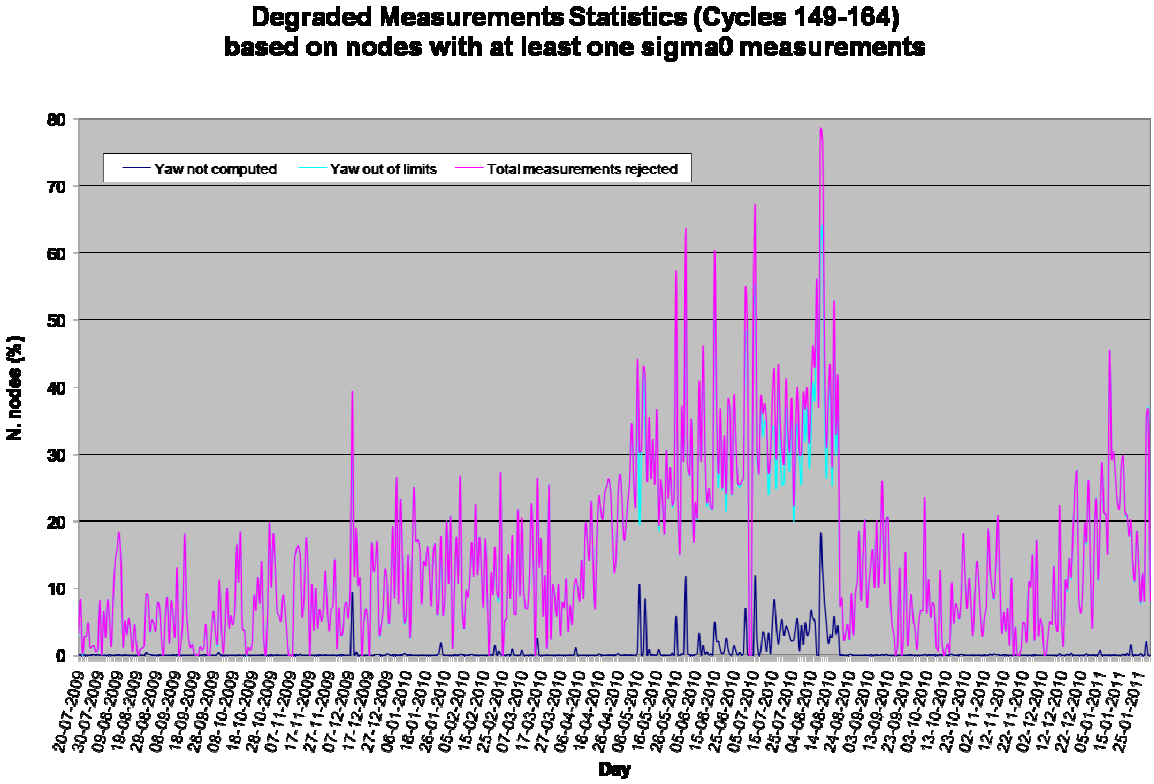

FIGURE 32 Statistics of sigma nought degraded measurements.

The statistics are also computed based on sea and land nodes. For these statistics the analysis is based on the valid triplets.

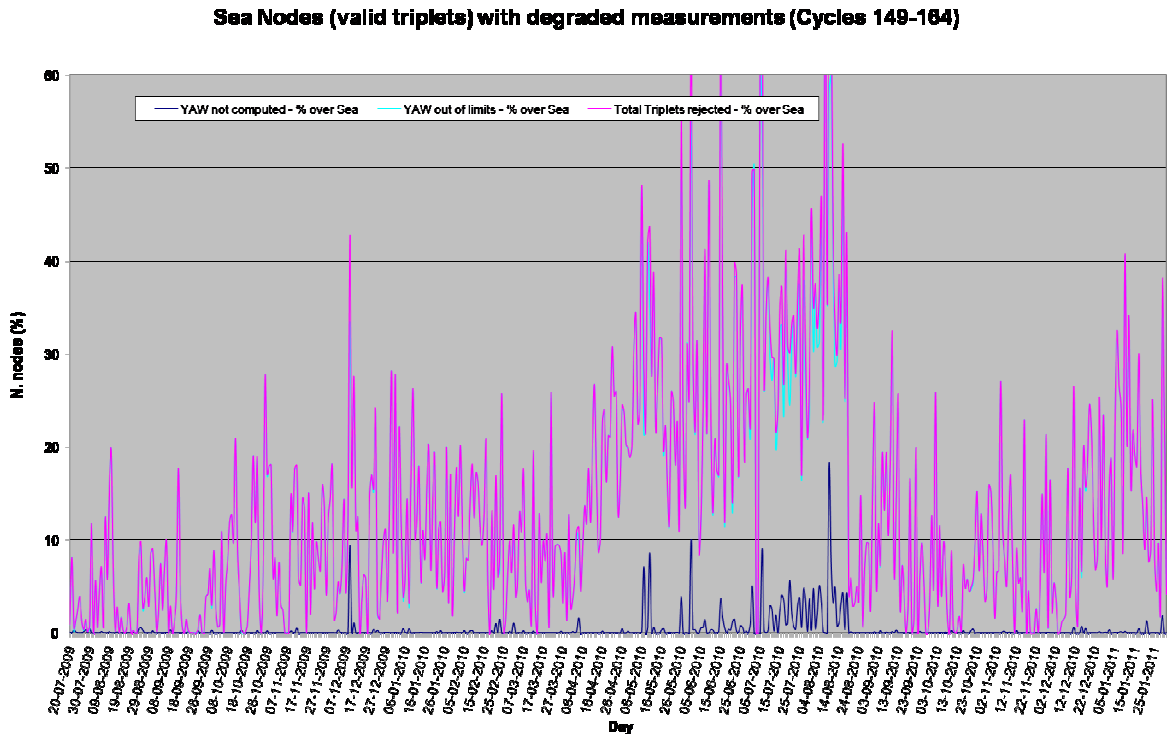

FIGURE 33 Statistics of degraded sigma nought triplets over Sea.

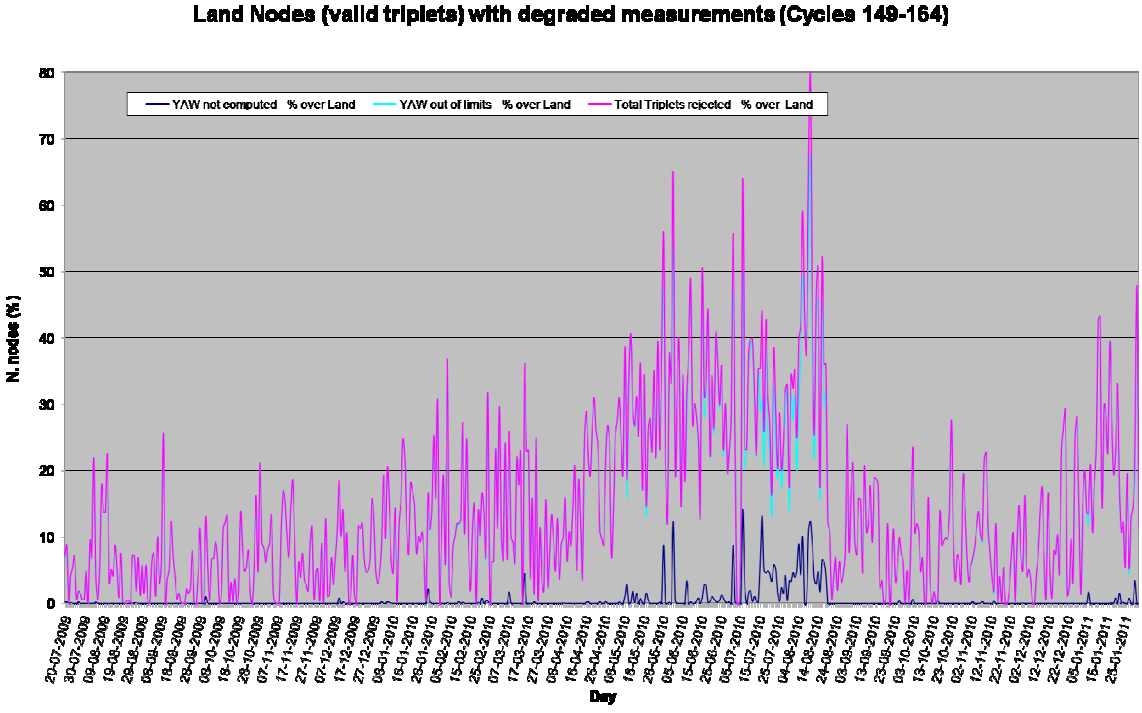

FIGURE 34 Statistics of degraded sigma nought triplets over Land.

Since the beginning of the analyzed period, the percentage of the degraded measurements was within 0-10% for most of the period. Peaks of degraded measurements on 8th and 9th August and from 12th to 14th September are caused by satellite attitude not corrected due to missing YAW statistics as a consequence of a ground segment dissemination problem. Peak on 10th September is due to missing YAW statistics caused by a long instrument switch-down. Peaks on 30th September, on 10th, 27th and 28th October can be caused by satellite attitude not corrected due to missing YAW statistics as a consequence of a ground segment dissemination problem. On 9th December a peak of degraded measurements was due to the DES blinded. Peak on 13th January was due to degraded attitude caused by the DES blinding. Peaks on 16th and 31st January and 9th February were caused by satellite attitude not corrected due to missing YAW statistics (consequence of a ground segment dissemination problem). From May to October 2010 a strong increase of the degraded measurements was recorded with a percentage of 30% and peaks of 50-60%. This was due to a degraded satellite attitude caused by a flight segment configuration problem. The problem was fixed on 18th August.

In the reporting period the percentage of the scatterometer degraded measurements is mostly within 30%.